Biophysical Chemistry 78 (1999) 43–68

Towards a better description and understanding of biomolecular solvation

Stefan Boresch, Sabine Ringhofer, Peter Höchtl, Othmar Steinhauser*

Institut für Theoretische Chemie und Molekulare Strukturbiologie, Universität Wien, Währingerstrasse 17, A-1090 Vienna, Austria

Received 2 July 1998; received in revised form 12 November 1998; accepted 23 November 1998

Abstract

We introduce a flexible framework for the correct description of the solvation of biological macromolecules, the *dielectric field equation* (DFE). The formalism permits the use of any combination of quantum mechanical (QM), molecular mechanical (MM) and continuum electrostatic (CE) based techniques. For the CE region a method that yields the electric field rather than the potential is outlined. The DFE formalism makes clear the need to consider and to calibrate a dielectric boundary region surrounding the simulation system. The details of how to do this are presented for the case of the Ewald summation method; the effects are demonstrated by calculations of the dielectric properties and the spatially resolved Kirkwood G-factor, $G_K(r)$, of TIP3P water. Computing the dielectric properties of a multi-component system provides a sensitive method to better understand the solvation of biological macromolecules. Towards this goal a rigorous analysis of the dielectric properties of solvated biomolecules based on a decomposition of the frequency-dependent dielectric constant (or susceptibility) of the full system is presented. The meaning of our approach is investigated, and the results of a first application are reported. Using the method of Voronoi polyhedra, the dielectric properties of the first two solvation shells and bulk water are compared by re-analyzing a 12-ns trajectory of a zinc finger peptide in water [Löffler et al. J. Mol. Biol. 270 (1997) 520]. It is found that the first shell behaves considerably different; in addition, there is a non-negligible contribution to the total susceptibility of the system from coupling between the protein and the bulk water phase, i.e. the water molecules not in the immediate vicinity of the solute. © 1999 Elsevier Science B.V. All rights reserved.

Keywords: Solvation; Biological macromolecules; Dielectric field equation; Dielectric properties

* Corresponding author. Tel.: +43 1 427752716; fax: +43 1 427752790; e-mail: os@mdy.univie.ac.at

PII: S0301-4622(98)00235-X

1. Introduction

Over the last 20 years the field of biomolecular simulation has evolved rapidly. After the initial efforts to make (classical) molecular mechanical (MM) force fields work even for biomolecular systems, the second decade has seen the results in the form of a large number of important and insightful applications. Algorithmic developments and the continuous increase of computer power constantly extend the limits of what is possible. For isolated biomolecules without solvent simulations in the microsecond regime are now practicable. These biologically relevant time scales are still beyond reach when solvation is treated at the full atomistic level of detail; the current state of the art is ≤ 50 ns. Therefore, any simplification which lowers the computational cost of describing biomolecular solvation is highly welcome. This explains the appeal of implicit (or partially implicit) solvation models, i.e. approaches in which explicit solvent molecules are replaced by a dielectric continuum [1–3]. However, the trade-off between gain in efficiency and loss of detail has to be weighed carefully. While continuum electrostatics (CE) based methods are usually sufficiently accurate at some distance away from the solute, the vicinity of the solvated biomolecule often requires an explicit treatment of at least the first solvation shell [4].

Consequently, biomolecular solvation is often described by a combination of explicit atomistic and implicit continuum models [5–7]. Mixed approaches, however, always pose the problem of having to tune or calibrate the different computational techniques. The situation is even more complex since nowadays quantum mechanical (QM) computations of core regions, such as the active site or co-factor of a biomolecule, are quite frequent [8–10]. Furthermore, QM calculations are often augmented directly by implicit solvation techniques as well [11–14]. Therefore, we really face the task of combining up to three distinct regions as illustrated in Fig. 1: a QM inner core, an MM region consisting of the biomolecular matrix, possibly including explicit solvent (water) shells, and a region in which CE is used. It would be helpful to have available one theoretical formalism suitable for all three methods. A major goal of this paper is to provide such a unified description based on what we refer to as the *dielectric field equation* (DFE). It constitutes a framework on which further theoretical developments, as well as practical implementations, can be based. An interesting consequence of the DFE is the need to consider a boundary region (cf. Fig. 1) to, qualitatively speaking, 'terminate' the electrostatic interactions 'properly'. The details of adjusting this boundary in combination with the Ewald summation method [15,16] are given, and illustrative simulation results are presented.

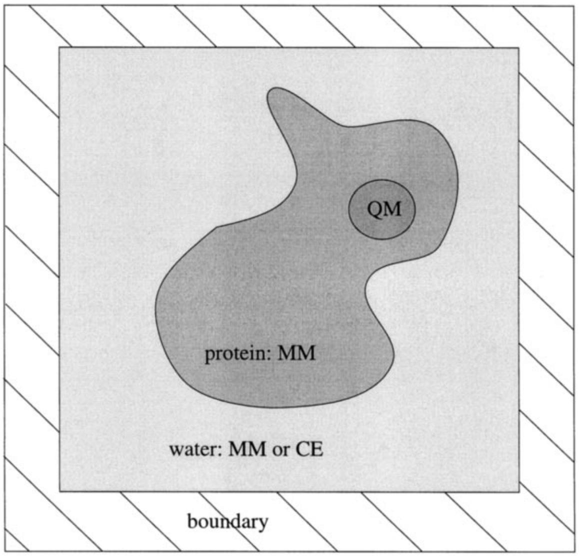

Fig. 1. Schematic representation of the methodological diversity that may be required for an accurate description of a protein in aqueous solution. A region of special interest, e.g. the active site, is treated quantum mechanically (QM); for the remainder of the protein, molecular mechanics (MM) is used. The solvent (water) is described by MM and/or continuum electrostatitics (CE). The simulation system (the inner box), consisting of QM, MM and CE region is embedded in a dielectric boundary that has to be considered as well (cf. Section 2.1.6).

These methodological issues are closely related to a better understanding of the biomolecule–water interface. A spatial resolution of the dielectric properties of the solvent, e.g. to compare the behavior of individual solvation shells, should prove insightful. Similarly, it is of interest to differentiate between outer (more hydrophilic) and inner (more hydrophobic) regions of the biomolecule. The importance of dielectric properties for stability and activity of proteins is well recognized [17] since they determine the complex charge screening occurring in protein and solvent [18]. A recent article gave an overview of the multiple important roles of electrostatic interactions in biology and chemistry [2]. A number of simulation studies investigating the dielectric properties of biomolecules have been reported in the literature; these include work by King et al. [19], Smith et al. [20], Simonson and co-workers [21–24], Yang et al. [25,26] and Löffler et al. [27].

Until recently, a fully worked out theoretical basis for the computation of dielectric properties from computer simulations existed only for homogeneous systems, i.e. molecular fluids. Solvated biomolecules are multicomponent systems; the presence of ions and of charged groups leads to additional complications. Löffler et al. [27] showed that potential problems resulting from this can be avoided by systematically distinguishing between contributions to the current (from charged components) and contributions to the dipole moment (from dipolar groups without net charge); the theory was then successfully applied to a simulation of HIV1 zinc finger peptide in water. Here we extend the methodology of Löffler et al. [27] to allow for an even finer decomposition of dielectric properties. In addition, we use the opportunity to present a more concise derivation of the theory and to carefully discuss the practical limitations and the meaning of such a ‘dielectric component analysis’. In an illustrative first application, we combine the theory with the method of Voronoi polyhedra to study the dielectric properties of the first two hydration shells of the HIV1 zinc finger peptide studied by Löffler et al. [27].

This paper is organized as follows. The theory section begins with the introduction of the DFE formalism and its application to QM, MM and CE; then the need for a boundary region is demonstrated (Section 2.1). In Section 2.2, it is shown how the boundary region can be calibrated when using the Ewald summation method [15,16]; this section can be regarded as a specialized application of the DFE. Section 3 contains the framework to study and decompose the dielectric properties of a biomolecule–solvent system; additional derivations are presented in Appendix A. We also report two sets of recent results that illustrate some of the theoretical considerations. In Section 4.1 we compare two simulations of TIP3P water with and without an adjusted dielectric boundary as described in Section 2.2. In Section 4.2 we report the dielectric properties of the first two solvation shells of HIV zinc finger peptide based on the simulation by Löffler et al. [27]. We conclude with a discussion of the results, as well as several suggestions for additional refinements and applications of the DFE formalism.

2. The dielectric field equation (DFE) — theory and an application

2.1. Describing solvation using the DFE framework

In this section we present a unified theoretical framework of biomolecular simulations in which a combination of methods based on QM, MM and CE is used. First, the DFE is introduced (Section 2.1.1). We then demonstrate that the formalism fulfills a number of requirements that make it appropriate for our purposes. As a prerequisite for its applicability we show that the DFE can be split into a sum of terms for different spatial regions that coincide with regions of different methodological description (Section 2.1.2). Next, the DFE formalism has to be flexible enough so that it can be adapted to QM, MM and CE. This is investigated in detail in Sections 2.1.3, 2.1.4 and 2.1.5, respectively. An often overlooked, but important contribution of the boundary region is studied next (Section 2.1.6), followed by a summary of the net equation for a system consisting of a QM, MM, CE, boundary region, and, possibly, an external field (Section 2.1.7).

2.1.1. Dielectric field equation (DFE)

Any interaction within and between molecules is electrostatic in nature, and so we focus on the Coulomb interaction

$$\varphi(\vec{r}) = \frac{1}{r}\,. \tag{1}$$

While in QM this follows from the Electrostatic Theorem [28], and while CE is exclusively based on electrostatics, the various energy terms of MM force fields (bond stretching, bond angle, dihedral terms, van der Waals term, etc.) in addition to Coulomb interactions may seem to contradict this. However, these 'non-electrostatic' terms result from the parameterization procedure that was carried out to avoid the full QM description. Furthermore, none of these terms cause practical problems due to the short range of their interactions. Nevertheless, we note that as far as MM is concerned we shall restrict our considerations to the explicit charge–charge, charge–dipole and dipole–dipole interactions.

In computer simulations one often deals with an electrostatic potential modified by a screening function $S(\vec{r})$ because of, e.g. the finiteness of the system; i.e. one has (in contrast to Eq. (1))

$$\varphi(\vec{r}) = \frac{1}{r} S(\vec{r}) \tag{2}$$

Throughout this paper, when we speak of Coulomb interactions and derived quantities (field, forces, dipole–dipole tensor), we always include the possibility of using Eq. (2) rather than Eq. (1).

A very general expression for the net electric field $\vec{E}(\vec{r})$ acting at a point $\vec{r}$ (which we shall show to be simultaneously applicable in QM, MM and CE) is given by the convolution integral

$$\vec{E}(\vec{r}) = \int_V \mathrm{d}\vec{r}' \Big\{ -\vec{\nabla}\varphi(\vec{r}-\vec{r}')\rho(\vec{r}') + \overleftrightarrow{T}(\vec{r}-\vec{r}')\vec{P}(\vec{r}') \Big\} \tag{3}$$

Eq. (3) is what we refer to as the *dielectric field equation* (DFE). The symbol $\rho(\vec{r})$ stands for a charge density; $\vec{P}(\vec{r})$ is a dipole density; $\varphi(\vec{r})$ has been defined in Eq. (2), and $\overleftrightarrow{T}(\vec{r})$ is the dipole–dipole tensor (the double gradient of the respective interaction potential)

$$\overleftrightarrow{T}(\vec{r}) = \vec{\nabla}\vec{\nabla}\varphi(\vec{r}). \tag{4}$$

The DFE follows directly from classical electrostatics as described, e.g. by Jackson [29]. (In fact, Eq. (3) is the gradient of Eq. (4.31) of [29]). Nevertheless, it contains three important generalizations. First, the bare Coulomb interaction (Eq. (1)) may be replaced by its modified analogue Eq. (2). Second, the respective densities $\rho(\vec{r})$ and $\vec{P}(\vec{r})$ have a rather different meaning depending on the type of method (QM, MM or CE) considered (this is investigated further in Sections 2.1.3, 2.1.4 and 2.1.5). Third, while in [29] the integration is carried out over all space, the volume of integration V has to be specified depending on the spatial or geometric boundary conditions used to make the DFE compatible with computer simulations, e.g. for periodic or toroidal boundary conditions (TBC), V is the volume of the central simulation box.

The convolution integral in Eq. (3) reflects the non-locality of the electric field. One can achieve locality, however, by Fourier transformation to reciprocal $\vec{k}$-space:

$$\tilde{\mathbf{E}}(\vec{k}) = \big(-\vec{\nabla}\varphi\big)(\vec{k})\,\tilde{\rho}(\vec{k}) + \tilde{\mathbf{T}}(\vec{k})\tilde{\mathbf{P}}(\vec{k}) \tag{5}$$

with appropriate expressions for all quantities

$$\tilde{\mathbf{E}}(\vec{k}) = \frac{1}{V}\int_V \vec{E}(\vec{r}) e^{i\vec{k}\cdot\vec{r}} \mathrm{d}\vec{r} \tag{6}$$

$$\tilde{\rho}(\vec{k}) = \frac{1}{V}\int_V \rho(\vec{r}) e^{i\vec{k}\cdot\vec{r}} \mathrm{d}\vec{r} \tag{7}$$

$$\tilde{\mathbf{P}}(\vec{k}) = \frac{1}{V}\int_V \vec{P}(\vec{r}) e^{i\vec{k}\cdot\vec{r}} \mathrm{d}\vec{r} \tag{8}$$

$$\tilde{\mathbf{T}}(\vec{k}) = \int_V \overleftrightarrow{T}(\vec{r}) e^{i\vec{k}\cdot\vec{r}} \mathrm{d}\vec{r} \tag{9}$$

Eq. (5), together with the definitions in Eqs. (6)–(9), is the DFE in reciprocal space. In passing, we note that the $\vec{k}=0$ limit of the above equations is equivalent to the global properties of the system, i.e. the spatial averages.

The various terms in Eqs. (1)–(9) fall into two groups with respect to time dependence. Clearly, $\rho(\vec{r})$, $\vec{P}(\vec{r})$ and $\vec{E}(\vec{r})$ depend on time, implicitly since $\vec{r}=\vec{r}(t)$, and also explicitly if an external field $\vec{E}_o(\vec{r},t)$ is present. On the other hand, in accord with QM and MM, the kernels $\vec{\nabla}\varphi(\vec{r}-\vec{r}')$ and $\overleftrightarrow{T}(\vec{r}-\vec{r}')$ are treated as time independent.

Since in this section external fields are of minor importance, and since molecular dynamics automatically takes into account the implicit time dependence of $\rho(\vec{r})$, $\vec{P}(\vec{r})$ and, hence, $\vec{E}(\vec{r})$, we ignore time dependence in the remainder of Section 2.

2.1.2. Volume decomposition

A QM description of a system consisting of a biomolecule (solute) and water (solvent) is impractical due to the computational effort involved; even when MM force fields are used the demands on computer resources quickly become prohibitively high for larger systems. As discussed in Section 1, this limitation is often circumvented by a combination of methods. A typical situation is depicted in Fig. 1, which schematically shows a biomolecule in water. A small region of the protein is treated by QM while the major part is handled by MM. The surrounding solvent is described either by MM or by a combination of MM and CE. In the latter case, one would treat the first layers of water explicitly by MM; bulk solvent is treated by CE [4]. The meaning of the boundary region encompassing the simulation system is discussed in Section 2.1.6. This division into regions is not primarily based on molecular components, but rather on spatial criteria. Atoms in the active site are handled differently than those in the rest of the biomolecule; waters may be subjected to MM or CE depending on the distance to the solute.

For the DFE to be useful, it has to be decomposable into separate terms for each computational technique employed according to spatially distinct regions (cf. Fig. 1 which was just discussed). This can be shown to be the case as follows. Let V_i denote the volume of such a region; i.e. the volume of the simulation system V becomes

$$V = \sum_i V_i. \tag{10}$$

Next, we introduce the three-dimensional step function

$$\Theta_{V_i}(\vec{r}) = \begin{cases} 1 & \vec{r} \in V_i \\ 0 & \vec{r} \ni V_i \end{cases} \tag{11}$$

Multiplying the charge or dipole density with the obvious identity

$$1 = \sum_i \Theta_{V_i}(\vec{r}), \tag{12}$$

a decomposition of $\rho(\vec{r})$ and $\vec{P}(\vec{r})$ into regions of uniform methodological treatment is readily achieved, i.e.

$$\rho(\vec{r}) = \sum_i \rho_i(\vec{r}) \tag{13}$$

$$\vec{P}(\vec{r}) = \sum_i \vec{P}_i(\vec{r}) \tag{14}$$

where we have used the regionally confined densities

$$\rho_i(\vec{r}) = \rho(\vec{r})\Theta_{V_i}(\vec{r}) \tag{15}$$

$$\vec{P}_i(\vec{r}) = \vec{P}(\vec{r})\Theta_{V_i}(\vec{r}) \tag{16}$$

Because of the linearity of the DFE, the additivity of the respective regional densities (Eqs. (15) and (16)) carries over into the DFE. Thus, we have shown that the DFE can be written as a sum of terms for different spatial regions. In practice, the volumes V_i will always coincide with regions of uniform methodological description.

2.1.3. Quantum mechanics (QM)

In this and the following two subsections, we define the meaning of $\rho_i(\vec{r})$ and $\vec{P}_i(\vec{r})$ for the three regions of particular interest, QM, MM and CE. The Electrostatic Theorem [28] based on the well-defined Born–Oppenheimer (BO) approximation [30], in combination with the Hellmann–Feynman Theorem [31], states that the fields acting on the nuclei in a molecule are determined by the Coulomb repulsion between nuclear charges and the mutual attraction between nuclear charges and the electron density:

$$\vec{E}(\vec{r}_I) = -\vec{\nabla}_I \left\{ \sum_{J=1}^{N} \frac{Z_J}{|\vec{r}_I - \vec{r}_J|} - \int \frac{\rho_{\mathrm{el}}(\vec{r})}{|\vec{r}_I - \vec{r}|} \mathrm{d}\vec{r} \right\} \tag{17}$$

Here the capitalized indices denote positions of the nuclei, the index I on the gradient operator indicates that the derivative is taken with respect to nucleus I; Z is the nuclear charge, and ρ_{el} is the electron density. Comparing Eq. (17) with the DFE (Eq. (3)) one obtains

$$\rho_{\mathrm{QM}}(\vec{r}) = \sum_J Z_J \delta(\vec{r} - \vec{r}_J) - \rho_{\mathrm{el}}(\vec{r}). \tag{18}$$

In the QM case, the charge density $\rho_{\mathrm{QM}}(\vec{r})$ consists of two contributions, the discrete charge distribution of the nuclei and the continuous electron density. The difficult term is, of course, $\rho_{\mathrm{el}}(\vec{r})$, which has to be computed for each nuclear geometry with one of the numerous standard quantum chemical methods [32,33]. We note that if nuclei-centered basis functions are used, so-called Pulay forces are necessary as well [34]. In the quantum mechanical region a dipole density $\vec{P}_{\mathrm{QM}}(\vec{r})$ cannot be meaningfully defined.

2.1.4. Molecular mechanics (MM)

The force (i.e. the negative gradient of the potential energy) is the central quantity of molecular dynamics (MD), as well as of minimization algorithms. It is related to the electric field $\vec{E}_i$ acting on an atom i by

$$\vec{F}_i^{\mathrm{el}}(\vec{r}) = q_i \vec{E}_i(\vec{r}). \tag{19}$$

This provides the connection between MM and the DFE formalism. The MM contribution to the field $\vec{E}$ is obtained by inserting the density of partial charges

$$\rho_{\mathrm{MM}}(\vec{r}) = \sum_j q_j \delta(\vec{r} - \vec{r}_j) \tag{20}$$

into the DFE (Eq. (3)).

It is sometimes advantageous to combine selected charges into a neutral charge group with dipole moment $\vec{\mu}_j = \Sigma_A q_A \vec{r}_{jA}$, in particular for solvent molecules. Thus, one can also define a dipolar density entering the DFE in the MM case

$$\vec{P}_{\mathrm{MM}}(\vec{r}) = \sum_j \vec{\mu}_j \delta(\vec{r} - \vec{r}_j). \tag{21}$$

Both $\rho_{\mathrm{MM}}(\vec{r})$ and $\vec{P}_{\mathrm{MM}}(\vec{r})$ are, of course, determined by the underlying force fields [35–37].

Eq. (21) is also valid for polarizable force-fields. In this case the $\vec{\mu}_j$ are not simply the dipole moments of charge groups, but there is an additional contribution $\vec{\mu}_{j,\mathrm{Pol}}$ following from the set of conditions

$$\frac{\partial U_{\mathrm{Pol}}}{\partial \vec{\mu}_{j,\mathrm{Pol}}} = 0 \quad \text{for all } j. \tag{22}$$

In other words, the dipole density consists of two contributions: a static permanent one due to the partial atomic charges plus the induced one due to dipole–dipole polarization [38–40].

2.1.5. Continuum electrostatics (CE)

As already mentioned in Section 1, we use the term continuum electrostatics loosely for any approach in which an explicit solvent is replaced by a dielectric continuum with a given dielectric constant ϵ_0. Although other techniques exist, such treatments are commonly associated with numerical solutions of the Poisson–Boltzmann (PB) equation [1,41–45]. These methods have found widespread applications and have extended our understanding of biomolecular systems; for a good overview see, e.g. Honig and Nicholls [2]. At the same time, approaches based on numerical solutions of the PB equation provide examples of the difficulties which arise when one attempts a combination with QM or MM-based methods. First, numerical differentiation is required to obtain the forces (i.e. the electric field), rendering in particular the combination with MD somewhat cumbersome. Second, instead of utilizing the precise positions of the charges in the non-CE region(s), they are distributed over the volume elements of the mesh. Third, no generalization to a modified Coulomb potential as described in Section 2.1.1

(Eq. (2) vs. Eq. (1)) is possible, presenting a separate difficulty concerning the adjustment to other regions.

In the remainder of this subsection we outline a CE approach which avoids some of these (potential) pitfalls. We first have to make clear the meaning of the charge density $\rho_{CE}(\vec{r})$ and the dipole density $\vec{P}_{CE}(\vec{r})$ in the CE region. While $\rho_{CE}(\vec{r})$ represents the net charge distribution of the cavity containing the QM and/or MM regions, i.e.

$$\rho_{CE}(\vec{r}) = \rho_{QM}(\vec{r}) + \rho_{MM}(\vec{r}) \tag{23}$$

$\vec{P}_{CE}(\vec{r})$ is the dielectric polarization of the CE region. It is related to the electric field via a non-local, constitutive relation

$$\vec{P}_{CE}(\vec{r}) = \int_V \chi(\vec{r}-\vec{r}')\vec{E}(\vec{r}')\mathrm{d}\vec{r}'. \tag{24}$$

The kernel of this convolution in space is the susceptibility $\chi(\vec{r}-\vec{r}')$. Note that $\vec{E}(\vec{r})$ is the electric field of all regions (QM, MM and CE) acting in the CE region. The susceptibility is related to a generalized dielectric constant (DC) or, more precisely, a dielectric response function $\epsilon(\vec{r}-\vec{r}')$ by [29]

$$\chi(\vec{r}-\vec{r}') = \frac{\epsilon(\vec{r}-\vec{r}') - \delta(\vec{r}-\vec{r}')}{4\pi}. \tag{25}$$

Fourier transformation makes the constitutive relation (Eq. (24)) local in reciprocal $\vec{k}$-space:

$$\tilde{\mathbf{P}}_{CE}(\vec{k}) = \tilde{\chi}(\vec{k})\tilde{\mathbf{E}}(\vec{k}) = \frac{\tilde{\epsilon}(\vec{k}) - 1}{4\pi}\tilde{\mathbf{E}}(\vec{k}) \tag{26}$$

As already mentioned in Section 2.1.1, the global, spatial averages correspond to the $\vec{k} = 0$ limit. For the dielectric polarization this spatial average is found to be the net dipole moment $\vec{M}$ divided by the net volume, i.e.

$$\tilde{\mathbf{P}}_{CE}(\vec{k} = 0) = \frac{1}{V}\int_V \vec{P}(\vec{r})\mathrm{d}\vec{r} = \frac{\vec{M}}{V} \tag{27}$$

Analogously, the dielectric response function

$$\tilde{\epsilon}(\vec{k} = 0) = \int_V \epsilon(\vec{r})\mathrm{d}\vec{r} \tag{28}$$

reduces to the global DC of the system ϵ_0

$$\tilde{\epsilon}(\vec{k} = 0) = \epsilon_0. \tag{29}$$

The last step makes clear the connection between the susceptibility $\chi(\vec{r}-\vec{r}')$ and $\chi(\vec{k})$ defined by Eqs. (24) and (26), and the traditional concept of a DC.

Eq. (3) and Eq. (24) form a coupled set of integral equations from which the dielectric polarization $\vec{P}_{CE}(\vec{r})$ induced by the charge distribution $\vec{\rho}_{CE}(\vec{r})$ (Eq. (23)) can, in principle, be computed. Using the corresponding equations in reciprocal space (Eq. (5) and Eq. (26)), one can readily obtain the formal solution

$$\tilde{\mathbf{P}}_{CE}(\vec{k}) = \left\{\mathbf{I} - \frac{\tilde{\epsilon}(\vec{k}) - 1}{4\pi}\tilde{\mathbf{T}}(\vec{k})\right\}^{-1} \left(-\vec{\nabla}\varphi\right)(\vec{k})\tilde{\rho}(\vec{k}) \tag{30}$$

where $\mathbf{I}$ is the unit tensor.

For Eq. (30) to be useful, however, one needs to have information about $\tilde{\epsilon}(\vec{k})$. To continue, we (have to) assume locality of the dielectric response function in real space

$$\epsilon(\vec{r}-\vec{r}') = \epsilon(\vec{r})\delta(\vec{r}-\vec{r}'). \tag{31}$$

Inserting Eq. (31) in Eq. (24) yields a local closure relation in real space

$$\vec{P}_{CE}(\vec{r}) = \frac{\epsilon(\vec{r}) - 1}{4\pi}\vec{E}(\vec{r}) \tag{32}$$

This last equation combined with the DFE (Eq. (3)) gives an approximate integral equation for the dielectric polarization $\vec{P}_{CE}(\vec{r})$,

$$\vec{P}_{CE}(\vec{r}) = \frac{\epsilon(\vec{r}) - 1}{4\pi}\int_V \mathrm{d}\vec{r}'\left\{-\vec{\nabla}\varphi(\vec{r}-\vec{r}')\rho_{CE}(\vec{r}') + \overleftrightarrow{T}(\vec{r}-\vec{r}')\vec{P}_{CE}(\vec{r}')\right\} \tag{33}$$

To solve Eq. (33), the following two steps are necessary: first, the field originating from the cavity charge distribution $\rho_{CE}(\vec{r})$ defined by Eq. (23),

$$\vec{E}_o(\vec{r}) = -\int_V d\vec{r}'\vec{\nabla}\varphi(\vec{r}-\vec{r}')\rho_{CE}(\vec{r}'), \tag{34}$$

is a constant input with regard to the computation of $\vec{P}_{CE}(\vec{r})$. Second, the singularity of the T-Tensor at the origin

$$\lim_{|\vec{r}|\to 0} \overleftrightarrow{T}(\vec{r}) = -\frac{4\pi}{3}\delta(\vec{r})\overleftrightarrow{I} \tag{35}$$

has to be taken into account when evaluating the second half of the integral in Eq. (33). Thus, one obtains the final integral equation for the dipole density $\vec{P}_{CE}(\vec{r})$

$$\vec{P}_{CE}(\vec{r}) = \frac{3}{4\pi}\frac{\epsilon(\vec{r})-1}{\epsilon(\vec{r})+2}\left\{\vec{E}_o(\vec{r}) \lim_{\sigma\to 0} \times \int_{|\vec{r}-\vec{r}|>\sigma} d\vec{r}'\overleftrightarrow{T}(\vec{r}-\vec{r}')\vec{P}_{CE}(\vec{r}')\right\} \tag{36}$$

where the limit makes clear the exclusion of the infinitesimal volume centered about the origin.

Eq. (36) can be solved by a combination of fast Fourier transform and iterative techniques (S. Boresch and O. Steinhauser, to be published). In practical applications one would set ϵ of the cavity (the region described by MM and/or QM) to some low value corresponding to the high frequency optical DC (which accounts solely for the electronic polarizability), and to the DC of water outside, completely analogous to PB methods.

2.1.6. Boundary region

So far, we have shown how the three computational methodologies (QM, MM and CE) considered here fit into and are described by the DFE framework. As discussed, Fig. 1 illustrates how they might be combined for the study of a solvated biopolymer. However, we have also depicted a region which surrounds the actual simulation system. To investigate whether such a *boundary region* is needed, we first give some plausibility arguments; then we show based on Maxwell's equations that a description without it would not be complete.

In contrast to all other regions discussed so far, the integration vector $\vec{r}'$ in the DFE (Eq. (3)) is not confined to a finite volume for such a boundary region. This suggests that for the boundary the following approximation is appropriate:

$$|\vec{r}-\vec{r}'| \approx |\vec{r}'| \tag{37}$$

Inserting this into the DFE leads to

$$\vec{E}_{hom} = \int\overleftrightarrow{T}(\vec{r}-\vec{r}')\vec{P}(\vec{r}')d\vec{r}' \approx \int\overleftrightarrow{T}(\vec{r}')\vec{P}(\vec{r}')d\vec{r}', \tag{38}$$

i.e. the boundary region contributes a constant, spatially homogeneous field. Since the simulation system contains all relevant charges in its QM and MM part (cf. Sections 2.1.3 and 2.1.4), it suffices to consider the dipole density for the boundary region.

However, the inconspicuous integral on the right hand side of Eq. (38) requires some care. It involves the integration of a long-ranged dipolar interaction over all space except for the inner core that is treated specifically by QM, MM and/or CE methods. The interaction decays as $1/r^3$ whereas the volume element of integration grows as r^2dr. The proper way to evaluate the integral is as follows. One starts with a finite volume V_0 and scales it by some parameter λ, i.e. $V = \lambda V_0$. The integration is carried out over this instantaneous volume and only afterwards the limit is taken, i.e.

$$\vec{E}_{hom} = \lim_{\lambda\to\infty}\int_{\lambda V_0}\overleftrightarrow{T}(\vec{r}')\vec{P}(\vec{r}')d\vec{r}' \tag{39}$$

Due to the long-range nature of dipolar interactions, however, this limit is not unique, but depends on the shape of the initial volume V_0 [46].

The procedure just outlined is equivalent to the computation of the $\vec{k} = 0$ Fourier component of the field, $\tilde{\mathbf{E}}(\vec{k} = 0)$. Therefore, the qualitative consideration presented in the previous paragraph suggests that there is an arbitrariness in the $\vec{k}=0$ Fourier component of the electric field, which cannot be resolved solely on mathematical grounds. This remaining mathematical arbitrariness is the underlying reason why a boundary region is required. To distinguish it from spatial or geometric boundary conditions (e.g. TBC), which are a common element of MD and Monte Carlo simulations, we refer to the boundary region also as the *dielectric boundary conditions*. Calibration of this dielectric boundary has to be based on physical considerations. A practical example of this for an important, special case (Ewald summation) is discussed in detail in Section 2.2 and pertinent simulation results are presented in Section 4.1.

The argumentation given so far has been qualitative. The possibility and need for a spatially homogeneous field contribution from the boundary region can be rationalized more exactly as follows: Irrespective of all possible or necessary decompositions into regions of different methodological treatment, the net electric field has to obey the Maxwell equations (cf. Jackson [29] for the special form used)

$$\vec{\nabla}\cdot\vec{E}(\vec{r}) = -4\pi\left\{\vec{\nabla}\cdot\vec{P}(\vec{r}) - \rho(\vec{r})\right\} \tag{40}$$

$$\vec{\nabla}\times\vec{E}(\vec{r}) = 0. \tag{41}$$

Since $\vec{E}(\vec{r})$ is a particular solution of these inhomogeneous partial differential equations, one can always augment it by a contribution from the corresponding homogeneous equation [47]

$$\vec{\nabla}\cdot\vec{E}(\vec{r}) = 0 \tag{42}$$

that simultaneously fulfills Eq. (41). This is true regardless whether one considers an infinite system or a finite system under TBC. Clearly, a spatially homogeneous field as suggested by Eq. (38) fulfills Eq. (41) and Eq. (42).

2.1.7. Net equation and external field

Finally, we allow for the possibility that the whole system is exposed to an external electric field. The most general form of $\vec{E}(\vec{r})$ consists, therefore, of the sum of all regional fields, the homogeneous contribution of the boundary region $\vec{E}_{\mathrm{hom}}$ and the external field $\vec{E}_0$

$$\vec{E}(\vec{r}) = \sum_i \vec{E}_{V_i}(\vec{r}) + \vec{E}_{\mathrm{hom}} + \vec{E}_0 \tag{43}$$

with the regional fields

$$\vec{E}_{V_i}(\vec{r}) = \int_V \mathrm{d}\vec{r}'\Big\{-\vec{\nabla}\varphi(\vec{r}-\vec{r}')\rho_i(\vec{r}') + \vec{\vec{T}}(\vec{r}-\vec{r}')\vec{P}_i(\vec{r}')\Big\} \tag{44}$$

originating from the respective regional charge and dipole densities discussed in Sections 2.1.3, 2.1.4 and 2.1.5. Note that the volume of integration for the regional contributions to the field is the full volume V as discussed for Eq. (3), not just that of the respective region.

2.2. Adjustment of dielectric boundary conditions

In Section 2.1.6 the need to embed the simulation system in a boundary (cf. Fig. 1) was shown to be one element of a more correct description of solvated systems. We consider this step as the adjustment of dielectric boundary conditions, which should be distinguished from geometric or spatial boundary conditions, such as TBC (cf. Section 2.1.6 and [47]). When using the Ewald summation, which is rapidly becoming the method of choice to simulate solvated biomolecular systems [48,49], this calibration is straightforward to accomplish. The full details have been published by Boresch and Steinhauser [50]; here we give a shortened summary that emphasizes how the adjustments follow from and fit into the DFE framework.

The Ewald potential [15,16], aside from constant terms that do not contribute to the electric field, can be written in the form

$$\varphi_{\mathrm{EW}}(\vec{r}) = \frac{1}{r}S_{\mathrm{EW}}(\vec{r}) = \frac{1}{r}\Big\{ erfc(\eta r)$$

$$+r\sum_{\vec{k}\neq 0}\frac{4\pi}{VK^2}e^{(-k^2/4\eta^2)}\cos\left(\vec{k}\cdot\vec{r}\right)\Bigg\},\tag{45}$$

which reflects that it is an example of a modified Coulomb potential as discussed in Section 2.1.1. Eq. (45) is a particular solution of the Poisson equation under periodic or toroidal boundary conditions (TBC) [47]. The parameter η controls the relative weight of the two terms; $\vec{r}$ is a Cartesian position vector; r is an inter-particle distance, and V is the volume of the central simulation box. For an introduction to the method, see, e.g. Allen and Tildesley [16]. The sum in Eq. (45) runs over discrete reciprocal lattice vectors $\vec{k} = (2\pi n_x/a,\ 2\pi n_y/b,\ 2\pi n_z/c)$, where a, b and c are the dimensions of the simulation box and n_x, n_y, $n_z = 0,1,2,\ldots$.

The development given in Section 2.1 leading to Eq. (43) makes clear that φ_{EW} can always be augmented by

$$\varphi_{\mathrm{EW,hom}}(\vec{r}) = -\vec{r}\cdot\vec{E}_{\mathrm{hom}}.\tag{46}$$

Since $\vec{E}_{\mathrm{hom}}$ is intimately related to the $\vec{k}=0$ term of the DFE (cf. Eq. (5)) as discussed in detail in Section 2.1.6, we need to consider the properties of the term $\tilde{\mathbf{T}}(\vec{k}=0)\tilde{\mathbf{P}}(\vec{k}=0)$. From Eq. (27) we have $\tilde{\mathbf{P}}(\vec{k}=0)=\vec{M}/V$, and it can be shown that for isotropic systems the T-tensors of the modified Coulomb potentials commonly used in MD simulations (cutoff, reaction field, Ewald) are a multiple of the unit tensor in the $\vec{k}=0$ limit [51–53]. Therefore, a suitable choice for $\vec{E}_{\mathrm{hom}}$ is an expression analogous to a spherical reaction field (RF) [16,54]

$$\vec{E}_{\mathrm{hom}} = \frac{4\pi}{3}\lambda_{\mathrm{RF}}\frac{\vec{M}}{V} = \vec{E}_{\mathrm{RF}}\tag{47}$$

with

$$\lambda_{\mathrm{RF}} = \frac{2(\epsilon_{\mathrm{RF}}-1)}{2\epsilon_{\mathrm{RF}}+1}.\tag{48}$$

Here ϵ_{RF} is the (formal) DC of the surrounding medium (the boundary region of Fig. 1) giving rise to the RF; however, V and $\vec{M}$ are the volume and the net dipole moment of the simulation system as opposed to the volume and dipole moment of a sphere with cut-off radius r_c centered on the reference particle in the traditional spherical RF [16,54]. While the field $\vec{E}_{\mathrm{RF}}$ fulfills TBC, the corresponding potential (Eq. (46)) does not. Nevertheless, since periodicity of the field is the physically relevant condition [47], Eq. (47) is a valid functional form for $\vec{E}_{\mathrm{hom}}$ in Eq. (43) that can be added to the standard Ewald potential, as first proposed by de Leeuw et al. [15].

This, in principle, well known result forms the basis on which the adjustment of dielectric boundary conditions relies. However, upon proceeding one has to take into account that the Ewald summation already contains an *intrinsic* RF, $\vec{E}^{\mathrm{intr}}_{\mathrm{EW,hom}}$, which can be shown to be [52]

$$\vec{E}^{\mathrm{intr}}_{\mathrm{hom,EW}} = \frac{4\pi}{3}\lambda_{\mathrm{EW}}\frac{\vec{M}}{V}\tag{49}$$

with

$$\lambda_{\mathrm{EW}}(\eta,r_c) = \int_0^{r_c} 4\pi r^2 \mathrm{d}r \left(\frac{\eta}{\sqrt{\pi}}\right)^3 e^{-\eta^2 r^2}.\tag{50}$$

The upper limit of integration, r_c, is the cutoff radius used in the calculation of the real space part of the Ewald sum (first term of Eq. (45)). The parameter λ_{EW}, which typically has values very close to unity for reasonable choices of η and r_c, can be related to a formal Ewald DC ϵ_{EW} of the boundary region by the following transformation of variables

$$\epsilon_{\mathrm{EW}}(\eta,r_c) = \frac{2+\lambda_{\mathrm{EW}}}{2(1-\lambda_{\mathrm{EW}})}\tag{51}$$

or vice versa

$$\lambda_{\mathrm{EW}} = \frac{2(\epsilon_{\mathrm{EW}}-1)}{2\epsilon_{\mathrm{EW}}+1}\tag{52}$$

Comparison of Eq. (52) with Eq. (48) makes clear the formal similarity of λ_{EW} and λ_{RF} and justifies the interpretation of $\vec{E}^{\mathrm{intr}}_{\mathrm{hom,EW}}$ as a RF. Eq. (52) maps the interval $0.95 < \lambda_{\mathrm{EW}} < 1$ onto the range $30 < \epsilon_{\mathrm{EW}} < \infty$. For a proper choice of η and r_c one has $\lambda_{\mathrm{EW}} = 1$ and $\epsilon_{\mathrm{EW}} = \infty$. Since an infinite DC corresponds to a conducting medium, such as a metal, this case is often denoted as *tinfoil* or *conducting* boundary conditions. Thus, in standard implementations of the Ewald summation the RF due to the dielectric boundary corresponds to a DC $\epsilon_{\text{hom}} = \epsilon_{\text{EW}} = \infty$ since $\vec{E}_{\text{hom}} = E^{\text{intr}}_{\text{hom,EW}}$. This well established result demonstrates that the absence of an explicit term for $\vec{E}_{\text{hom}}$ in the method used to compute the Coulomb interactions (i.e. the Ewald summation in this case) is not equivalent to having omitted or avoided the dielectric boundary conditions. In addition, note that ϵ_{EW} and, consequently, $\vec{E}^{\text{intr}}_{\text{hom,EW}}$ are determined by the two simulation parameters η and r_c and not by physical considerations.

Any physically meaningful boundary region should provide a smooth transition from the atomistic description in the simulation system to the continuum description of the surrounding medium. Thus, when averaging the atomistic, spatially inhomogeneous field acting in the simulation cell, the resulting macroscopic field should correspond to the intrinsic DC ϵ_0 of the simulated system itself. Once one understands the intrinsic contribution of the Ewald method, it is straightforward to adapt $\vec{E}_{\text{hom}}$ to the more physical situation $\epsilon_{\text{hom}} = \epsilon^{eff}_{EW} = \epsilon_0$. One combines the (unphysical) contribution intrinsic to the Ewald method, $\vec{E}^{\text{intr}}_{\text{hom,EW}}$, with an additional, explicit RF

$$\vec{E}_{\text{add}} = \frac{4\pi}{3}\lambda_{\text{add}}\frac{\vec{M}}{V} \tag{53}$$

that can be used for calibration. Overall, there is an effective reaction field

$$\vec{E}_{\text{hom}} = \vec{E}^{\text{eff}}_{\text{hom,EW}} = \vec{E}^{\text{intr}}_{\text{hom,EW}} + \vec{E}_{\text{add}} = \frac{4\pi}{3}\lambda^{\text{eff}}_{\text{EW}}\frac{\vec{M}}{V} \tag{54}$$

Since all terms in Eq. (54) have the functional form of a RF, the effective field strength $\lambda_{\text{hom}} = \lambda^{eff}_{EW}$ is given by

$$\lambda^{\text{eff}}_{\text{EW}} = \frac{2(\epsilon_{\text{EW}} - 1)}{2\epsilon_{\text{EW}} + 1} + \lambda_{\text{add}} = \frac{2(\epsilon^{\text{eff}}_{\text{EW}} - 1)}{2\epsilon^{\text{eff}}_{\text{EW}} + 1}, \tag{55}$$

where $\epsilon^{\text{eff}}_{\text{EW}}$ is the effective Ewald DC. In contrast to λ_{EW} or, equivalently, ϵ_{EW}, which are functions of η and r_c, λ_{add} is a freely tunable parameter, and $\epsilon^{\text{eff}}_{\text{EW}}$ can be adjusted to values selected on physical grounds. For the particular choice $\epsilon^{eff}_{EW} = \epsilon_0$ and ideal tinfoil conditions ($\lambda_{\text{EW}} = 1$) the strength λ_{add} of the additional RF $\vec{E}_{\text{add}}$ is given by

$$\lambda_{\text{add}} = -\frac{3}{2\epsilon_0 + 1} \tag{56}$$

Eq. (53) combined with Eq. (56) allows one to adjust the dielectric boundary conditions of a simulation in which Ewald summation is used to $\epsilon^{\text{eff}}_{\text{EW}} = \epsilon_0$, i.e. the dielectric constant of the boundary region is the same as that of the simulated system.

3. Decomposition of dielectric properties

In this section we show how dielectric properties of biomolecular systems can be analyzed based on a decomposition of the $\vec{k} = 0$ limit (see below) of the frequency-dependent DC $\epsilon(\omega)$ or of the frequency-dependent susceptibility $\chi(\omega)$, which are related by

$$4\pi\chi_i(\omega) = \epsilon_i(\omega) - 1. \tag{57}$$

Aside from an outline of the theory, the emphasis of this section is on how such a ‘dielectric component analysis’ has to be understood and interpreted. The detailed derivations based on linear response theory (LRT), including the generalizations necessary for additional ionic components, can be found in Appendix A.

In the derivation and discussion of the DFE (Section 2.1) explicit time dependence was of minor importance since the focus was on internal molecular fields, i.e. the intra- and intermolecular interactions in the simulation system. The dielectric properties of biomolecules in solution can be measured as the response of the system to an in general time-dependent external field. Analogously, the theoretical formalism (i.e. LRT) used to study dielectric properties is based on a time-dependent external field (even though no such field may be present in the actual simulations

[16]). Thus, in the following we have to take time dependence into account explicitly.

The heterogeneity of solvated biomolecular systems suggests to search for a decomposition of the overall dielectric properties, i.e. to define DCs for various regions of interest of both solute and solvent as depicted in Fig. 2. In this illustration, we distinguish between inner and outer regions of the protein (hydrophobic core vs. more hydrophilic surface), as well as the first two solvent layers as opposed to bulk water. We stress that regions of particular interest during analysis in general do *not* coincide with the regions of differing methodological treatment in the DFE formalism; i.e. the meaning of Figs. 1 and 2 should be carefully discerned. However, there is an even more fundamental difficulty with any approach based directly on Fig. 2. One sees this immediately when considering the most general definition of the dielectric susceptibility [46]

$$\vec{P}(\vec{r},t) = \int_V \chi(\vec{r}-\vec{r}',t-t')\vec{E}(\vec{r}',t')\mathrm{d}\vec{r}'\mathrm{d}t'. \tag{58}$$

Eq. (58) is the generalization of Eq. (24) if time dependence is important, as is the case here. The

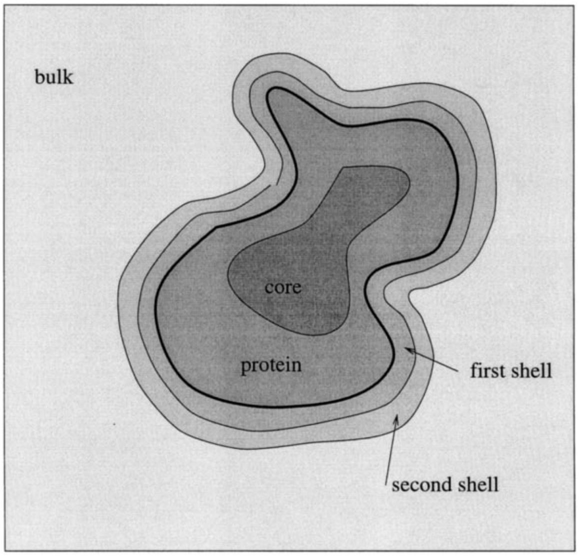

Fig. 2. Regions of interest for understanding the dielectric properties of a solvated protein. In the example shown, the hydrophobic core, outer regions of the protein, two solvation shells and bulk water are distinguished.

non-locality of $\chi(\vec{r}-\vec{r}',\ t-t')$ makes it impossible to use regional susceptibilities defined in analogy to the regional charge and dipole densities of the DFE framework (Eqs. (15) and (16)); i.e. in general, one cannot write

$$\chi_i(\vec{r}) \neq \chi(\vec{r})\Theta_{V_i}(\vec{r}). \tag{59}$$

To make $\chi(\vec{r}-\vec{r}',\ t-t')$ local, one has to carry out a Fourier transformation in both space and time, leading to the generalization of Eq. (26)

$$\tilde{\mathbf{P}}(\vec{k},\omega) = \tilde{\chi}(\vec{k},\omega)\tilde{\mathbf{E}}(\vec{k},\omega). \tag{60}$$

In $\vec{k}$-space component-specific, individual susceptibilities $\tilde{\chi}_i(\vec{k},\omega)$ which add up to the net susceptibility of the system can be introduced without any ambiguity; i.e.

$$\tilde{\chi}(\vec{k},\omega) = \sum_i \tilde{\chi}_i(\vec{k},\omega) \tag{61}$$

In principle, this decomposition of the susceptibility or dielectric properties may proceed up to any granularity, provided the respective component behaves like a dielectric material. The most interesting quantity is the $\vec{k}=0$ term which corresponds to the global (spatially averaged) quantities; therefore, in the following we shall only consider $\tilde{\chi}(\vec{k}=0,\omega) = \chi(\omega)$ and, similarly, $\tilde{\chi}_i(\vec{k}=0,\omega) = \chi_i(\omega)$. Nevertheless, this $\vec{k}=0$ limit should not be confused with locality in r-space.

The origin of the non-locality of component-specific susceptibilities becomes clear from the full statistical mechanical derivation presented in Appendix A. There, the exact definition of a component DC ϵ_i is given by Eq. (84) which is related to χ_i by Eq. (57). All derivations in Appendix A are based on Ewald summation with adjusted dielectric boundary conditions (cf. Section 2.2). Since the emphasis of this section lies on understanding the meaning of χ_i and on working out its essential features, we specialize to conducting boundary conditions (i.e. we set $\epsilon_{\mathrm{EW}}^{\mathrm{eff}} = \infty$ in Eq. (84) of Appendix A). In this case (which corresponds to the most frequently used dielectric boundary condition in practical calculations) the component-specific susceptibility simplifies to:

$$\chi_i(\omega) = \sum_j \chi_{ij}(\omega) \tag{62}$$

with the pair susceptibility $\chi_{ij}(\omega)$ given by

$$\chi_{ij}(\omega) = \frac{1}{3Vk_bT} L\left[-\dot{\Phi}_{ij}\right]. \tag{63}$$

Here k_b is the Boltzmann constant, T the temperature, and $\Phi_{ij}(t)$ is the time correlation function between the total dipole moments $\vec{M}_i(t)$ and $\vec{M}_j(t)$ of two respective regions considered, i.e.

$$\Phi_{ij}(t) = \langle \vec{M}_i(0) \cdot \vec{M}_j(t) \rangle. \tag{64}$$

The symbol $L[f]$ denotes the Fourier–Laplace transform of the function f

$$L[f] = \int_0^\infty \mathrm{d}t e^{-i\omega t} f(t) \tag{65}$$

and $\dot{f}(t) = \mathrm{d}f/\mathrm{d}t$ as usual.

One sees from Eq. (62) that even in $\vec{k}$-space there is coupling between the formally additive dielectric components $\chi_i(\vec{k}=0,\omega)$ defined by Eq. (61). Each χ_i contains a self-term χ_{ii} which comes from the autocorrelation function Φ_{ii}, as well as cross-terms χ_{ij} related to the cross-correlation functions Φ_{ij}. While there is exactly one Φ_{ii} per component susceptibility χ_i, the cross-term contributions are shared among all components considered. This becomes especially clear when one specializes the general equation for a two-component system consisting of, e.g. a protein (label P) and water (label W). In this case the two dipolar correlation functions of interest are

$$\Phi_{\mathrm{P}}(t) = \Phi_{\mathrm{PP}}(t) + \Phi_{\mathrm{PW}}(t) = \langle \vec{M}_{\mathrm{P}}(0) \cdot \vec{M}_{\mathrm{P}}(t) \rangle + \langle \vec{M}_{\mathrm{P}}(0) \cdot \vec{M}_{\mathrm{W}}(t) \rangle \tag{66}$$

$$\Phi_{\mathrm{W}}(t) = \Phi_{\mathrm{WW}}(t) + \Phi_{\mathrm{PW}}(t) = \langle \vec{M}_{\mathrm{W}}(0) \cdot \vec{M}_{\mathrm{W}}(t) \rangle + \langle \vec{M}_{\mathrm{P}}(0) \cdot \vec{M}_{\mathrm{W}}(t) \rangle. \tag{67}$$

Both expressions contain the autocorrelation contribution accounting for the protein–protein and water–water dipolar correlations, respectively, as well as a shared cross-term $\langle \vec{M}_{\mathrm{P}}(0) \cdot \vec{M}_{\mathrm{W}}(t) \rangle$ which describes the coupling between the two spatially distinct regions. The susceptibility of the protein χ_{P} (and, consequently, the DC of the protein ϵ_{P}) contains a contribution which originates from the dipolar coupling between P and W; the same term contributes to χ_{W} (ϵ_{W}). By straightforward generalization (cf. also Eqs. (62)–(64)) it is clear that the susceptibility of a specific region depicted in Fig. 2, e.g. the first layer of solvent, contains coupling contributions from all other regions.

Considering Eqs. (62), (66) and (67) makes clear that it is problematic to interpret a component susceptibility χ_i as the intrinsic susceptibility of this particular region. Instead, Eq. (61) allows one to understand how individual regions contribute to the total susceptibility of the system, i.e. to permit some interpretation and understanding what gives rise to the overall dielectric properties. Furthermore, one gains insights into self-term (Φ_{ii}) compared to cross-term contributions ($\Phi_{ij,j\neq i}$) to Φ_i, and, thus, to the formal dielectric components χ_i or ϵ_i (cf. Eq. (62) and the previous paragraph).

The limiting case of infinite dilution behaves as expected if the proposed decomposition (Eq. (61)) is understood as just described. Since the Fourier–Laplace transform is linear, a component susceptibility χ_i is always proportional to Φ_i; i.e. it follows from Eq. (63) that

$$\chi_i \propto \frac{1}{V} \Phi_i. \tag{68}$$

We consider again the two component system consisting of protein P and water W. As we go to more and more dilute solutions, $\Phi_{\mathrm{P}}(t)$ will tend towards a limiting value independent of the volume V; hence, $\lim_{V\to\infty} \chi_{\mathrm{P}} \to 0$. Since the same is true for the cross-term contribution to χ_{W}, the only non-vanishing contribution is the water–water self-term; in other words, the dielectric properties of the system resemble more and more those of bulk water, as expected.

Differences in the time or frequency dependence of the component susceptibilities $\chi_i(\omega)$ can provide further insights into the overall dielectric behavior of the system. The mobility of dipolar components, such as bulk water, bound surface water, and residues at the surface and in the core of a biopolymer is expected to vary significantly. If the differences in mobility are large enough, they will result in a multi-modal frequency distribution of the overall dielectric susceptibility $\chi(\omega)$. The formalism introduced here permits the decomposition of $\chi(\omega)$ into components as a function of the frequency, and, hence, differences in mobility are reflected in the frequency dependence of these components $\chi_i(\omega)$. Therefore, while the 'dielectric component analysis' presented here is not suited for a classification of dielectric properties based on spatial regions, it, nevertheless, allows one to understand the frequency dependence of $\chi(\omega)$ in full microscopic detail.

4. Recent pertinent results

4.1. Adjustment of dielectric boundary conditions

4.1.1. Methodological details

The effects of choosing $\epsilon_{EW}^{eff} \approx \epsilon_0$ compared to $\epsilon_{\mathrm{EW}}^{\mathrm{eff}} = \infty$ were studied by computing the dielectric properties of the transferable interaction potential three point (TIP3P) water model [55]. In particular, the behavior of the distance-dependent Kirkwood G-factor $G_K(r)$ was investigated. TIP3P is one of the most often employed water models in biomolecular simulations [36,37,56]. Surprisingly, different values for its static DC can be found in the literature. Chipot et al. [57] reported a DC of 96, whereas Simonson [58] obtained a value of 82, using the microscopic droplet model. A recent detailed study from our group (in which, however, only tinfoil boundary conditions were employed) found a DC of 97 [59].

The static DC ϵ_0 of a homogeneous fluid can be obtained from MD simulations based on Eq. (80) of Appendix A (cf. also [50,51]). The spatial resolution of dipolar correlations is of special interest; for the case of a homogeneous dipolar liquid, such as water, it is best described by the spatial decomposition of the Kirkwood G-factor, $G_K(r)$, defined as

$$G_K(r) = \langle \hat{\vec{\mu}}_i \cdot \hat{\vec{M}}(r) \rangle \tag{69}$$

where

$$\hat{\vec{M}}(r) = \sum_{r_{ij} \le r} \hat{\vec{\mu}}_j \tag{70}$$

and $\hat{\vec{\mu}}_i(r)$ denotes a unit vector in the direction of the dipole moment of molecule i. $G_K(r)$ describes the angular correlation of a reference dipole $\hat{\vec{\mu}}_i$ with all its peers within a sphere of radius r. Intuitively, one expects that beyond some threshold R_0 all dipolar correlations vanish and that $G_K(r)$ reaches a plateau value typical for a continuum region. This means that if one rewrites $G_K(r)$ as

$$G_K(r) = G_K(R_0) + \int_{R_0}^{V} \vec{\mu} \cdot \vec{P}(\vec{r}) \mathrm{d}\vec{r}, \tag{71}$$

the second term should not contribute. This will be examined for the two types of dielectric boundary conditions considered.

Since the majority of existing results for the DC of TIP3P suggests a value close to 100, the dielectric boundary conditions in the simulation with the additional RF term were adjusted to this value. Two simulations with ($\epsilon_{\mathrm{EW}}^{\mathrm{eff}} = 100$) and without ($\epsilon_{\mathrm{EW}}^{\mathrm{eff}} = \infty$) the additional, explicit RF term defined by Eq. (53) and Eq. (56) were carried out, and the DC, as well as the r-dependent G-factor $G_K(r)$, were computed. The same self-written MD program employed by Boresch and Steinhauser [50] was utilized; most technical details of the simulations were the same as described there. Only calculations with a traditional implementation of the Ewald summation were carried out. The length of the simulation was 3 ns in the case of tinfoil boundary conditions and 1.5 ns for the run with the adjusted boundary conditions.

4.1.2. Results

The dielectric properties of TIP3P water as obtained from the two simulations described above are summarized in Table 1. The two values

Table 1
Dielectric properties of TIP3P water[a]

	EW[b]	EW-RF[c]
ϵ_0[d]	100.(10)	106.(10)
τ[e]	6.1	5.9

[a]Results are corrected for the respective influence of the dielectric boundary condtions.
[b]Obtained from simulations with tinfoil boundary conditions.
[c]Obtained from simulations with adjusted dielectric boundary conditions.
[d]Static dielectric constant.
[e]Relaxation time of the system dipole moment in picoseconds.

for the static DC of TIP3P [100 without RF-term (i.e. tinfoil boundary conditions) and 106 with the RF-term (i.e. adjusted dielectric boundary conditions)] lie well within the estimated statistical error bars of 10, as they must, since computer adapted dielectric theory [51] accounts for the use of different dielectric boundary conditions. The result is in good agreement with Chipot et al. [57] and Höchtl et al. [59]. The relaxation times of the system dipole moment (obtained from a mono-exponential fit of the dipole–dipole time autocorrelation function and corrected for the different dielectric boundary conditions [51]) are 6.1 ps (without RF) and 5.9 ps (with RF), respectively.

By contrast, the spatial resolution of G_K, i.e. $G_K(r)$, which is plotted in Fig. 3, reveals the differences in dipolar correlations resulting from the two choices of dielectric boundary conditions. While in both cases the interaction of a water dipole with its first, second and third coordination shell can be seen at approximately 3.7, 6.0 and 8.5 Å, respectively, there are large quantitative differences. As seen from Eq. (71), one expects no further correlation beyond a certain threshold, such as the third coordination shell. However, in the calculation with tinfoil boundary conditions $G_K(r)$ continues to rise. The simulation in which $\epsilon_{\mathrm{EW}}^{\mathrm{eff}} = \epsilon_0$, on the other hand, is in line with expectation. Beyond 10 Å only minor fluctuations in $G_K(r)$ can be observed. Fig. 3 clearly demonstrates that the use of tinfoil boundary conditions leads to the presence of artificial dipolar density $\vec{P}(r)$ beyond local structure (Eq. (71)). For the

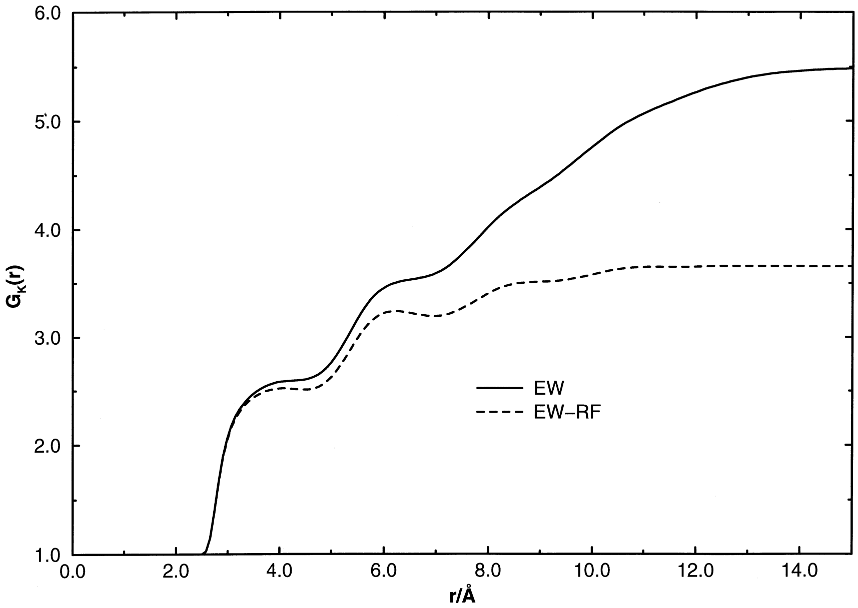

Fig. 3. The spatially resolved Kirkwook G-factor, $G_K(r)$, of a system of TIP3P water as a function of the dielectric boundary conditions used. EW (solid line) denotes tinfoil boundary conditions, i.e. $\epsilon_{\mathrm{EW}}^{\mathrm{eff}} = \infty$; EW-RF (dashed line) stands for the case $\epsilon_{\mathrm{EW}}^{\mathrm{eff}} = 100$.

fairly small system used here, differences between the two dielectric boundary conditions are already discernible for the first solvation shell. This influence on even local dipolar correlation becomes less pronounced for larger systems; the asymptotic behavior for large distances, however, remains.

In principle, the importance of dielectric boundary conditions should be clear from the fact that a computer-adapted dielectric theory is needed in the first place [51]. However, the computation of dielectric properties (of homogeneous systems) from MD simulations works so well (cf., e.g. [50,60] and the results presented here) that the role of the boundary may have become obscured since the theoretical framework for the analysis compensates the influence of the boundary used during the simulation. Furthermore, tinfoil boundary conditions require no explicit term due to $\vec{E}_{\mathrm{hom}}$ in the force calculation, which might lead one to believe that no boundary is present. We stress that $\epsilon_{\mathrm{EW}}^{\mathrm{intr}} = \infty$ corresponds to one particular dielectric boundary condition as revealed by the influence this choice has on $G_K(r)$ (see Fig. 3).

The present results, as well as those of Boresch and Steinhauser [50], make clear the influence of dielectric boundary conditions. Ewald summation with tinfoil boundary conditions results in artificial dipolar correlations at large distances. We stress, however, that it is, in our opinion, currently the best generally applicable method to handle electrostatic interactions in computer simulations using TBC. The calibration outlined here requires some generalizations if ionic compounds are present. In this case the straightforward application of Eq. (53) becomes problematic since contributions of free charges $q_i\vec{r}_i$ to the net dipole moment are discontinuous when an ion crosses the surface of the basis cell and is subjected to TBC [25,47]. We refer the reader to Section 2.1.4 of Boresch and Steinhauser [50] for the details. Calculation of $\vec{E}_{\mathrm{add}}$ based on the current rather than the dipole moments as suggested there need to be tested; then careful simulation studies will be necessary to see whether the differences in dipolar correlations also have structural (and/or dynamical) effects. Orientational correlation functions (which are related to $G_K(r)$ [59]) should provide a sensitive probe, and they are equally applicable to multi-component systems [61].

4.2. Dielectric properties of the first two solvation shells of a protein

4.2.1. Motivation

Löffler et al. [27] recently studied the dielectric properties of a system consisting of a small protein (HIV1 zinc finger peptide), water and two Cl^- counter-ions. The frequency-dependent DC contributions of the protein and of water, as well as the conductivity of the ions were separated and analyzed. It was found that the coupling of the current (zinc plus the two Cl^- counter-ions) to the dipole moment of the other components was very small and could be neglected in practice. Thus, the results of Löffler et al. [27] essentially correspond to the two-component model (protein P and water W) used in Section 3 to illustrate some of the theoretical considerations. For water (ϵ_{W}), the self-term resulted in a static DC of 44, this value increased slightly to 47 if the cross-term (coupling to the protein) was included. The same cross-term also contributes to ϵ_{P} (Eqs. (66) and (67)); there the relative effect was much more important: the static DC was 12 without coupling and 15 with coupling, a difference of 20%.

Section 3 and Appendix A make clear that a decomposition of dielectric properties need not be restricted to large scale 'natural' boundaries, such as protein and water, but can be made finer, in accord with the inherent inhomogeneity of biomolecular systems. For example, the properties of water bound to the surface of the protein would be of interest since they are known to behave quite differently from bulk water [62]. A further subdivision of the solvent, e.g. into hydration shells of bound water and more flexible water molecules outside, requires an appropriate algorithm for spatial decomposition. Although a number of concepts exist which describe the first hydration shell by suitably chosen pair distribution functions [63], or which divide the biopolymer into spherical shells about some center [21–24], these methods introduce additional parameters with not always obvious physical meaning. Furthermore, they do not cover the entire space, but only some preferred regions. The method of Voronoi polyhedra is an attractive alternative, which is free of such parameters [64,65]. It was applied in an earlier study from this group which also investigated the properties of surface vs. bulk water [62]. Among other related quantities, Abseher et al. [62] computed the single particle correlation function of the dipole moment of water molecules in the first two solvation shells. It was found that water in the vicinity of the protein behaves very differently from bulk water. The single particle dipole–dipole time correlation functions are localized properties which only depend on the immediate vicinity of the reference particle. Since one can average over a large number of particles, good statistics are easily obtained. This makes it a highly appropriate quantity to distinguish between bound and free water. However, it has nothing to do with the highly non-local dielectric properties considered here, which depend on the net dipole moment of a spatial region including its coupling to all other regions of the system. To illustrate the type of results possible by a combination of the generalized theory presented in Section 3 with the method of Voronoi polyhedra, we present here first data of a re-analysis of the zinc finger–water system described above [27] in which the dielectric properties of the first two solvent shells were compared to that of bulk water.

4.2.2. Methods

Our analysis is based on a 12-ns trajectory of an 18 residue neutral zinc finger peptide [66] in a periodic box ($45 \times 45 \times 45$ Å) of 2872 SPC/E [67] water molecules. The protocol for the MD simulation has been described in detail in [27]. (In the original study a 13.1-ns calculation was carried out, but data equivalent to approximately 1 ns were corrupted.)

The method of Voronoi polyhedra was used for the decomposition of the solvent into solvation shells and a bulk phase. It was carried out with two programs from the 'code-mbg' library [65,68]. In accord with the results of the study by Abseher et al. [62] discussed above, only the first two water shells were treated separately; the remaining waters were considered as bulk. The shells were constructed as follows. In a first step, all water oxygens in contact with the protein were identified. Then, the Voronoi volumes for this first water shell (including both oxygens and hydrogens) were computed. The second shell was defined analogously as all waters in contact with the first solvent layer.

The Voronoi analysis is quite time consuming, so the trajectory was processed in increments of 1 ps; i.e. altogether 12 000 data points were extracted. This is appropriate since the correlation times of interest vary from apprroximately 10 ps (water) up to > 2000 ps (protein) [27]. Denser sampling would have resulted in a somewhat more detailed resolution of the various correlation functions for short times, but the most important limitation is the insufficient length (!) of even a 12 or 13-ns trajectory.

To avoid some of these problems we also considered the contributions to the static DC, i.e. the $\omega = 0$ case. It can be obtained directly from Eq. (63) using $L[\dot{\Phi}_{ij}(\omega = 0)] = \langle \vec{M}_i \cdot \vec{M}_j \rangle$. For this preliminary analysis the various time correlation functions $\langle \Phi_{ij}(t) = \vec{M}_i(0) \cdot \vec{M}_j(t) \rangle$ of the regional dipole moments $\vec{M}_i(t)$ and $\vec{M}_j(t)$, where i and j stand for protein, first and second water shell, and
bulk water, respectively, were least-square fitted to a bi-exponential decay $A_1 \exp(-t/\tau_1) + A_2 \exp(-t/\tau_2)$, following [27]. Further manipulations were based on these fitted functions; in particular, all Fourier–Laplace transforms were carried out analytically. (For some cross-correlation functions, no meaningful fit could be obtained; these cases are discussed in Section 4.2.3.) Since the MD simulation used Ewald summation with tinfoil boundary conditions [27], the component susceptibilities were evaluated according to Eq. (63).

4.2.3. Results

As just described, we investigated the dielectric properties of four regions using the method of Voronoi polyhedra in the present study: the protein (P), the first and the second solvation shell (labelled S1 and S2, respectively) and the remaining water, i.e. bulk (B). Both the static, as well as the frequency-dependent contributions to the overall susceptibility (or dielectric constant) of the system were analyzed.

Table 2 lists all static properties ($\omega = 0$), the pair susceptibilities χ_{ij} (obtained as described in Section 4.2.2), the component contributions χ_i (written in italics) and the overall susceptibility χ (in boldface). To facilitate the comparison with the dielectric constant, all susceptibilities in Table 2 are multiplied by 4π (the connection between susceptibilities and dielectric constants is given by Eq. (57)). The sum of one row (or column) of χ_{ij}-values is the respective component contribution χ_i (Eq. (62)). Similarly, the χ_i-components add to the total susceptibility χ of the system (Eq. (61)). In addition, Table 2 contains the average Voronoi volumes of the four regions (rightmost column).

The first row (or column) of Table 2 lists the four pair susceptibilities (χ_{P-P}, χ_{P-S1}, χ_{P-S2} and χ_{P-B}) that yield the contribution $\chi_P = 13.4$ of the protein to the overall susceptibility of the system. The cross-correlations of the protein with the shells are very small ($\chi_{P-S1} = -0.3$ and $\chi_{P-S2} = 0.3$) and can be neglected. Between the protein and the bulk there exists a non-negligible cross-correlation ($\chi_{P-B} = 2.8$) which amounts to 24% of the self-term ($\chi_{P-P} = 10.6$). The magnitude of the cross-terms is directly proportional to the size of the time average $\langle \vec{M}_P \cdot \vec{M}_j \rangle$, where $j = \{S1,S2,B\}$. Thus, the size of the contributions from the three cross-terms reflects first that the dipole moment of B is much larger than that of the two shells. This is in agreement with the average volumes of the three regions (rightmost column in Table 2). On the other hand, it is interesting to note that there is so little correlation between P and the two shells; furthermore, χ_{P-S1} and χ_{P-S2} exactly compensate each other.

Table 2
The static pair susceptibilities χ_{ij}, component susceptibilities χ_i and overall susceptibility χ of HIV1 zinc finger peptide in aqueous solution[a]

χ_{ij}	P[b]	S1[c]	S2[d]	B[e]	χ_i[f]	V_i[g]
P	10.6	−0.3	0.3	2.8	*13.4*	2510
S1	−0.3	2.3	0.3	0.5	*2.8*	6096
S2	0.3	0.3	3.9	1.4	*5.9*	11 118
B	2.8	0.5	1.4	32.5	*37.2*	71 399
χ_i	*13.4*	*2.8*	*5.9*	*37.2*	**59.3**[h]	

[a]All susceptibilities are multiplied by 4π to facilitate comparison to component DCs.
[b]Protein.
[c]First shell.
[d]Second shell.
[e]Bulk water.
[f]Obtained as the column or row sum of the χ_{ij}.
[g]Average Voroni volumes of the components in Å^3.
[h]Sum of all component susceptibilities, i.e. $\chi = \Sigma_i \chi_i$.

All pair susceptibilities involving the two shells, including the self-terms (i.e. χ_{ii}), are fairly small. Nevertheless, a few interesting observations can be deduced from Table 2. Coupling between the two shells, as reflected by χ_{S1-S2} is very weak (0.3). Compared to the self-terms, the coupling of S2 with B is slightly stronger than that of S1. Both findings are in accord with the expected different behavior of waters in the first shell compared to bulk water. By contrast, little can be concluded regarding the second shell from the static results alone.

The bulk makes the dominant contribution ($\chi_B = 37.2$) to the overall susceptibility of the system ($\chi = 59.3$). This is, of course, a consequence of our decomposition approach. The bulk region occupies by far the largest volume; hence, its contribution to χ has the largest weight. Its relative contribution would increase further for higher dilutions, as it must (cf. Section 3). The non-negligible coupling with the solute (the protein) reflected by $\chi_{P-B} = 2.8$ was already discussed.

The frequency-dependent pair and component susceptibilities provide information about the dynamic behavior. To compute them in a straightforward manner, one has to be able to fit the respective dipole moment time correlation functions $\Phi_{ij}(t)$ (Eq. (64)) to a functional form for which the Fourier–Laplace transform (Eq. (65)) can be carried out analytically. As described above, we so far have only attempted to model the $\Phi_{ij}(t)$ by a bi-exponential decay. This worked well for the self-terms $\Phi_{ii}(t)$, but failed for several cross-correlation functions. On the other hand, the contributions to the static overall susceptibility χ from the $\chi_{ij,i \neq j}$ were very small (see Table 2), with the exception of the coupling between P and B. Since this one cross-term, which obviously is of interest, could be fitted by a bi-exponential function, we decided to ignore the other cross-terms at this stage. We are aware that it may not be fully justified to neglect coupling between S2 and B (cf. Table 2), but this correlation function could not be fitted to a bi-exponential function. Thus, in the following we consider only the four self-term contributions $\chi_{P-P}(\omega)$, $\chi_{S1-S1}(\omega)$, $\chi_{S2-S2}(\omega)$ and $\chi_{B-B}(\omega)$, as well as the P–B cross-term, $\chi_{P-B}(\omega)$.

Since susceptibilities are essentially Fourier–Laplace transforms, they always have a real and imaginary part, i.e. $\chi(\omega) = \chi'(\omega) + i\chi''(\omega)$. The information contained in the two parts is equivalent as can be seen from the Kramers–Kronig relation [69]. In the present case the interesting features are easier to distinguish in the imaginary susceptibilities $\chi_{ij}''(\omega)$. These are shown in Fig. 4. Since a number of details are difficult to discern at this scale, Fig. 5 contains a magnified view of $\chi_{S1-S1}''(\omega)$, $\chi_{S2-S2}''(\omega)$ and $\chi_{P-B}''(\omega)$. The spectrum of the total susceptibility $\chi''(\omega)$, which is also included in Fig. 4, shows two well-separated peaks. From the component spectra, one can immediately distinguish between the maximum at lower frequencies ($\omega_{P,max} \approx 2 \cdot 10^{-4}$ ps^{-1}) resulting from the protein and the water peak ($\omega_{W,max} \approx 10^{-1}$ps^{-1}). One sees in Fig. 4 that the protein peak in $\chi''(\omega)$ is not only due to $\chi_{P-P}''(\omega)$, but is influenced by the protein–bulk cross-term (short-dashed line in Fig. 4) as well. This is reflected by an increase in height of the protein peak in the overall spectrum $\chi''(\omega)$ (thick line) accompanied by a shift towards higher frequencies compared to the protein–protein spectrum (long-dashed line). In Fig. 5 an enlarged view of $\chi_{P-B}''(\omega)$ is presented; in this plot the position of the maximum due to the protein in the overall frequency-dependent susceptibility is indicated as a thin solid line.

The decomposition of the water component into bulk water and two solvation shells shows that the contribution of bulk water dominates both the magnitude of the peak, as well as the location of its maximum. Inspecting the contributions of the two shells reveals that the location of $\chi_{S1-S1}(\omega_{max})$ is at significantly lower frequencies compared to the bulk peak, so that even the total water peak is shifted towards lower frequencies

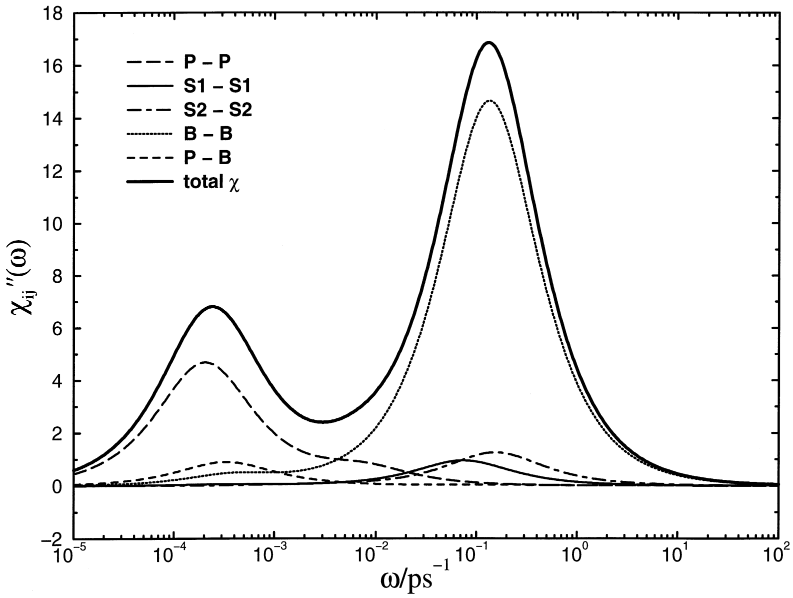

Fig. 4. Imaginary part of the frequency-dependent susceptibility $\chi_{ij}''(\omega)$ multiplied by 4π. P stands for protein, S1 for the first, S2 for the second solvation shell, and B for bulk water. The total susceptibility of the system $\chi''(\omega)$ is shown as well (thick solid line).

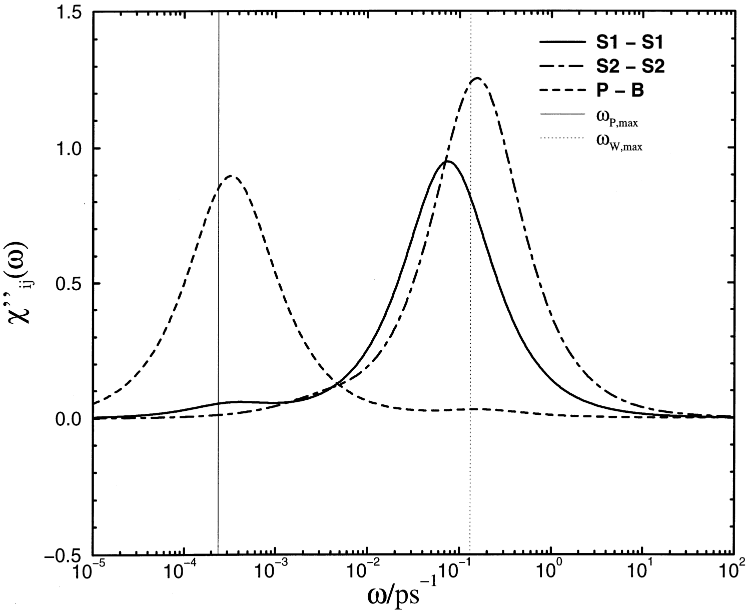

Fig. 5. Enlarged plot of $\chi_{S1-S1}''(\omega)$, $\chi_{S2-S2}''(\omega)$ and $\chi_{P-B}''(\omega)$ defined in Fig. 4. The position of the two maxima in the total susceptiblity $\chi''(\omega)$ is indicated by the two vertical lines.

despite the small relative weight of the S1-phase (cf. again the average volumes in Table 2). The peak in the spectrum of the second shell lies at about the same frequency as that of bulk water. The magnified plot (Fig. 5) clearly shows the differences between χ_{S1-S1}'' and χ_{S2-S2}''. Their position relative to the cumulative water peak in $\chi''(\omega)$ is made clear by the thin, dotted line indicating the position of $\chi''_{max,W}$.

A number of conclusions can be drawn from these first results. The first solvation shell can be clearly distinguished from bulk water. By contrast, the dielectric properties of S2 already resemble those of the bulk phase. However, a small, but non-negligible influence from the interaction between the protein and the bulk phase (i.e. only those waters not in the immediate vicinity of the protein) could be discerned, both in the static contribution, as well as in the frequency-dependency of the total susceptibility. The results illustrate how a ‘dielectric component analysis’ can aid in understanding the overall dielectric behavior of the full system.

5. Summary, discussion and outlook

We have presented two related contributions relevant to the study of solvated macromolecules by computer simulations. The DFE framework introduced in Section 2 connects several computational methodologies (QM, MM, CE) and provides the theoretical basis for a more accurate description of solvated biomolecules. The need to adjust dielectric boundary conditions follows from the DFE approach, and this was illustrated by a study of the spatially resolved dipolar correlations in TIP3P water [55]. The theory required for a decomposition of the dielectric properties of multicomponent systems, a generalization of the earlier work by Löffler et al. [27], was presented as well. First results of an application to a system consisting of a small protein in aqueous solution compared the dielectric behavior of the first two solvation shells and bulk water.

The last years have seen many important improvements in QM, MM and CE. Combined applications of these three methodologies become more and more frequent to help address the ever-increasing challenging problems of computational chemistry and molecular biology. We propose the DFE formalism as an aid in managing some of the difficulties that arise when employing them together. It makes clear the common elements of QM, MM and CE treatments and permits the use of modified Coulomb interactions, as is often necessary in practical work. The DFE shares this last characteristic with the computer-adapted dielectric theory of homogeneous liquids [51]. Both are adaptations of the general theory [29,46] to the special situation encountered in computer simulations. The somewhat atypical point of view presented here with respect to QM may prove helpful in combined approaches (see below). For the CE regime, an orthogonal approach to the ubiquitous PB methods [1,41–45] was outlined. While not in the least intended to replace PB calculations, which have amply demonstrated their utility, the derivations show that a CE treatment more consistent with QM and MM methods exists. The approach outlined here is based on the electric field rather than the potential, and, in accord with the general DFE formalism, modified electrostatic interactions are straightforward to incorporate.

Perhaps the most interesting consequence following from the DFE framework concerns the combination of CE and QM methods. In current QM calculations the need to account for the surrounding (dielectric) environment is gradually being recognized. Most frequently, a spherical cavity in combination with a multipole expansion is employed [5,6,13]; coupling with PB methods is also possible [70]. The CE treatment outlined here provides the basis for an alternative: Just as the charge density ρ_{QM} of the QM region directly enters the suggested CE approach, the dipole density P_{CE} can be fed back into the QM region as follows: from Eq. (40) one sees that $-\nabla \cdot \vec{P}_{\mathrm{CE}}$ is equivalent to a charge density which can be interpreted as a ligand field. Using standard techniques (i.e. pseudo nuclei as in standard ligand field theory), a corrected quantum mechanical solution can be obtained. The respective converged solutions for the field of the QM and the CE regions are then obtained by repeating the steps just outlined; in other words, another self-consistent-field cycle is added to the iterative procedures already required for both the QM and the CE treatment.

It is of interest to compare the principles of combining QM and CE just discussed to coupling of MM and CE within the DFE formalism. For pairwise additive force fields [35–37], the MM contribution is evaluated as usual. Then ρ_{MM} serves as the input for the CE method, similarly to the QM case; the resulting field from CE is added to the net field (cf. Eq. (43)). There is no further interaction between the two methods. This changes for polarizable MM force fields since in this case the CE solution affects the MM region. The corrected MM charge density has to be fed back into CE, until converged solutions are obtained in both regions. Thus for polarizable MM force fields coupled to a CE region, there is a high degree of analogy to the combination of QM and CE, as also observed in [14].

The results of the re-analysis of a 12-ns trajectory of a zinc finger peptide in aqueous solution [27] show the type of information that can be obtained from a combination of the generalized computer adapted dielectric theory presented here and the method of Voronoi polyhedra. The differences between the first solvation shell and bulk water could be clearly discerned. While most cross-terms were small, there was a non-negligible contribution from coupling between the protein and the bulk water phase. This emphasizes the non-locality of the component susceptibilities, and we repeat that the $\epsilon_i(\omega)$ cannot be equated with an intrinsic DC of the respective region.

The present analysis is only preliminary since it is limited by the use of a bi-exponential decay function for all dipole–dipole time correlation functions. Because of this, the frequency dependence of the various contributions to the dielectric constant are effectively modeled by only two parameters, potentially obscuring subtle details. Furthermore, a few cross-correlation functions could not be fitted at all; however, their contributions are expected to be small. Considering that little is known about the behavior of such cross-correlation functions, various functional forms of fitting functions, as well as numerical Fourier–Laplace transforms of the raw data will have to be compared carefully for a final analysis. These studies are currently being carried out.

Acknowledgements

We thank Gerald Löffler for technical assistance and acknowledge help by Siegfried Höfinger. This work was funded by the Austrian 'Fond zur Förderung der wissenschaftlichen Forschung' under the project number P-12537-CHE.

Appendix A: Theoretical basis of a dielectric component analysis

This Appendix contains the detailed derivations of the steps required to decompose the dielectric properties of a solvated biomolecule, including charged groups and ions. It complements Section 3.

A.1. Global dielectric properties of dipolar systems

We first give a summary of the relevant results from computer-adapted dielectric theory of molecular liquids [51]. Any time-dependent external field $\vec{E}_0(t)$ may be resolved in Fourier components

$$\vec{E}_0(t) = \int \mathrm{d}\omega e^{i\omega t}\vec{E}_0(\omega), \tag{72}$$

and linear response theory (LRT) allows the separate calculation of each frequency component. It suffices to consider a spatially homogeneous field since we are only interested in the $\vec{k}=0$ limit of the response (cf. Section 3). The polarization $\vec{P}(\vec{k}=0,\omega)$ induced by a spatially homogeneous external field $\vec{E}_0(t)$ in a system having volume V and temperature T is given by

$$\vec{P}(\vec{k}=0,\omega) = \frac{1}{3Vk_bT}L[-\dot{\Phi}]\vec{E}_0(\omega) \tag{73}$$

As in Section 3, $\Phi(t)$ is the time correlation function of the system dipole moment $\langle \vec{M}(0)\cdot \vec{M}(t)\rangle$; the dot denotes the derivative with respect to time, and the Fourier–Laplace transform $L[f]$ was defined in Eq. (65). The macroscopic counterpart of this microscopic result from LRT is the so-called constitutive relation [29]

$$\begin{aligned}\vec{P}(\vec{k}=0,\omega) &= \chi(\vec{k}=0,\omega)\vec{E}(\vec{k}=0,\omega)\\ &= \frac{\epsilon(\vec{k}=0,\omega)-1}{4\pi}\vec{E}(\vec{k}=0,\omega)\end{aligned} \tag{74}$$

Eq. (74) is the $\vec{k}=0$ limit of Eq. (60). The frequency-dependent susceptibility $\chi(\vec{k}=0,\omega)=\chi(\omega)$, or, alternatively, the frequency-dependent DC $\epsilon(\omega)$ are a unique material constant of the system. Combination of Eqs. (73) and (74) leads to

$$(\epsilon(\omega)-1)\vec{E}(\vec{k}=0,\omega) = \frac{4\pi}{3}\frac{1}{Vk_bT} \times L[-\dot{\Phi}]\vec{E}_0(\vec{k}=0,\omega) \tag{75}$$

The relation between the external field $\vec{E}_0$ and the Maxwell field $\vec{E}$, i.e. the $\vec{k}=0$ limit of the field acting in the simulation system as defined by Eqs. (6) and (43), was shown to be [51]

$$\vec{E}(\vec{k}=0,\omega) = \frac{3}{\epsilon(\omega)+2} \times\left(1-\frac{3}{4\pi}\frac{\epsilon(\omega)-1}{\epsilon(\omega)+2}\overleftrightarrow{T}(\vec{k}=0)\right)\vec{E}_0(\omega) \tag{76}$$

Here $\overleftrightarrow{T}(\vec{k}=0)$ is the spatially averaged (i.e. $\vec{k}=0$) T-Tensor defined by Eq. (9) for the (possibly modified) Coulomb potential φ (cf. Section 2.1.1). Next, we insert the T-Tensor appropriate for the Ewald summation method with adjusted dielectric boundary conditions (cf. discussions and derivations in Section 2.2 and Neumann and Steinhauser [52]).

$$\overleftrightarrow{T}(\vec{k}=0) = \frac{4\pi}{3}\frac{2(\epsilon_{\mathrm{EW}}^{\mathrm{eff}}-1)}{2\epsilon_{\mathrm{EW}}^{\mathrm{eff}}+1}\overleftrightarrow{I}, \tag{77}$$

where $\overleftrightarrow{I}$ is the unit tensor. In passing, we note that an identical expression holds for the spherical reaction field when $\epsilon_{\mathrm{EW}}^{\mathrm{eff}}$ is replaced by ϵ_{RF}.

Thus, upon combination of Eqs. (73), (74), (76) and (77), one obtains the final expression

$$(\epsilon(\omega)-1)\frac{2\epsilon_{\mathrm{EW}}^{\mathrm{eff}}+1}{2\epsilon_{\mathrm{EW}}^{\mathrm{eff}}+\epsilon(\omega)}=\frac{4\pi}{3}\frac{1}{Vk_bT}L[-\dot{\Phi}] \tag{78}$$

Eq. (78) is the sought after connection between the frequency-dependent DC $\epsilon(\omega)$ of the probe, i.e. the simulated system, and the time correlation function $\Phi(t)$ of the total dipole moment $\vec{M}$, a quantity that can be obtained from the simulation.

The static DC can be obtained as a special case of the general relation (Eq. (78)) for zero frequency. With

$$L[-\dot{\Phi}(\omega=0)]=\int_0^\infty \mathrm{d}t\left(-\frac{\mathrm{d}\Phi}{\mathrm{d}t}\right)=\langle M^2\rangle \tag{79}$$

one finds

$$(\epsilon(0)-1)\frac{2\epsilon_{\mathrm{EW}}^{\mathrm{eff}}+1}{2\epsilon_{\mathrm{EW}}^{\mathrm{eff}}+\epsilon(0)}=\frac{4\pi}{3}\frac{\langle M^2\rangle}{Vk_bT}. \tag{80}$$

which was used in Section 4.1. One clearly sees how the scaling factor $(2\epsilon_{\mathrm{EW}}^{\mathrm{eff}}+1)/(2\epsilon_{\mathrm{EW}}^{\mathrm{eff}}+\epsilon(0))$ accounts (and corrects) for the influence of different dielectric boundary conditions with respect to the computation of the static DC.

A.2 Dielectric component analysis

The results of the previous subsection (Eqs. (78) and (80)) were originally derived for the case of a homogeneous molecular fluid [51]. However, they are equally applicable to obtain the global dielectric properties of a multi-component (e.g. solute–solvent) system, provided that there are no ions or charged groups present, since in this case the net dipole moment is not uniquely defined [24,47,50]. Based on the work of Caillol and co-workers [71], the necessary generalization was given recently for a system consisting of a protein, solvent (i.e. water) and counter-ions [27]. Here we present a more concise derivation compared to Löffler et al. [27]. We first show that the formalism of the previous subsection can be extended to compute the contributions of individual regions of a dipolar multi-component system to the total DC; then we show how to handle complications due to the presence of ions or charged groups.

A.2.1. Dipolar components

The linearity of the LRT and of the constitutive relation makes possible the following decomposition of dielectric properties. Splitting the net polarization (Eq. (16)) as in the DFE formalism, one obtains immediately

$$\vec{P}_i(\omega)=\frac{1}{3Vk_bT}L\left[-\dot{\Phi}_i\right]\vec{E}_0(\omega), \tag{81}$$

as well as

$$\vec{P}_i(\omega)=\frac{\epsilon_i(\omega)-1}{4\pi}\vec{E}(\omega). \tag{82}$$

A few comments are in order. While LRT decomposition (Eq. (81)) may be done up to any desired granularity, application of the constitutive relation (Eq. (82)) is limited by the requirement that the respective region, for which an individual DC $\epsilon_i(\omega)$ is calculated, is large enough so that it behaves like a piece of dielectric material. The limits of granularity can only be determined by practical calculations, such as the results for the zinc finger peptide presented here (Section 4.2).

We continue by using the field relation (Eq. (76)) in combination with Eq. (77) as in the case of homogeneous systems (cf. also Appendix I of [27]). This last step is consistent with both the DFE framework and the definition of the $\chi_i(\vec{k},\omega)$, since we have

$$\tilde{\mathbf{P}}(\vec{k},\omega)=\sum_i\tilde{\chi}_i(\vec{k},\omega)\tilde{\mathbf{E}}(\vec{k},\omega)=\sum_i\tilde{\mathbf{P}}_i(\vec{k},\omega). \tag{83}$$

Eq. (83) follows from inserting Eq. (61) into Eq. (60), and it is the $\vec{k}$-space equivalent of the decomposition of the charge or dipole densities (Eqs. (15) and (16)) in r-space entering the DFE. One sees that the decomposition of the polarization requires the use of the Maxwell field of the full system in Eq. (82). Furthermore, it matches our ansatz for the decomposition of the susceptibilities introduced in Section 3 (Eq. (61)).

Thus, one finds the following expression for a DC component

$$(\epsilon_i(\omega)-1)\frac{2\epsilon_{\mathrm{EW}}^{\mathrm{eff}}+1}{2\epsilon_{\mathrm{EW}}^{\mathrm{eff}}+\epsilon(\omega)}=\frac{4\pi}{3}\frac{1}{Vk_bT}L\left[-\dot{\Phi}_i\right]. \tag{84}$$

with

$$\Phi_i(t)=\sum_{j=1}^{K}\Phi_{ij}(t)=\sum_{j=1}^{K}\langle\vec{M}_i(0)\cdot\vec{M}_j(t)\rangle. \tag{85}$$

With $\epsilon_{\mathrm{EW}}^{\mathrm{eff}}=\infty$ (tinfoil boundary conditions), Eqs. (84) and (85) simplify to Eq. (63) used in Section 3. Furthermore, the two equations are a generalization of an old result by Fröhlich. For the case $\omega=0$ (cf. Eq. (79)) and assuming (i) that $\epsilon_{\mathrm{EW}}^{\mathrm{eff}}=\epsilon(0)$; and (ii) that cross-terms are not important, Eqs. (84), (85) are equivalent to Eq. (7.43) of Fröhlich [72].

A.2.2 Additional ionic component

Biopolymers often contain charged groups which necessitate the addition of counter-ions to ensure electroneutrality. Complications related to this are also discussed in Boresch and Steinhauser [50], where it was shown that any ionic contribution to the system dipole moment has to be formulated as an integral over the net current. An analogous approach makes possible a generalization of the decomposition of dielectric properties for systems containing ions and charged groups. This is essential even for the study of global dielectric properties when charged groups are present.

Using the constitutive relation for the current density $\vec{j}(\omega)$

$$\vec{j}(\omega)=\frac{\vec{J}_I(\omega)}{V}=\sigma(\omega)\vec{E}(\omega) \tag{86}$$

and combining it with LRT one finds

$$\sigma(\omega)\frac{2\epsilon_{\mathrm{EW}}^{\mathrm{eff}}+1}{2\epsilon_{\mathrm{EW}}^{\mathrm{eff}}+\epsilon(\omega)}=\frac{4\pi}{3}\frac{1}{Vk_bT}L\left[\langle\vec{J}_I(0)\cdot\vec{J}_I(t)\rangle-\dot{\Phi}_I(t)\right]. \tag{87}$$

which connects the conductivity $\sigma(\omega)$ with the cross-correlation between ionic current $\vec{J}_I$ and dipolar contributions $\Phi_I(t)$, defined as

$$\Phi_I(t)=\sum_{j=1}^{K}\langle\vec{J}_I(0)\cdot\vec{M}_j(t)\rangle \tag{88}$$

To obtain the generalized expression for the individual DC in the presence of free ions or charged groups, three steps are required. First, the relationship between current J_I and dipole moment M_I

$$\vec{J}_I(t)=\dot{\vec{M}}_I \tag{89}$$

implies

$$\frac{\mathrm{d}}{\mathrm{d}t}\langle\vec{J}_I(0)\cdot\vec{M}_I(t)\rangle=\langle\vec{J}_I(0)\cdot\dot{\vec{M}}_I(t)\rangle=\langle\vec{J}_I(0)\cdot\vec{J}_I(t)\rangle \tag{90}$$

which explains why the current autocorrelation function, as well as the cross-correlation between current and dipolar components appear in Eq. (87). Furthermore, one also needs the following two identities

$$\langle\vec{J}_I(0)\cdot\vec{M}_j(t)\rangle=\langle\vec{J}_I(-t)\cdot\vec{M}_j(0)\rangle=\langle\dot{\vec{M}}_I(-t)\cdot\vec{M}_j(0)\rangle \tag{91}$$

and

$$\langle\dot{\vec{M}}_I(-t)\cdot\vec{M}_j(0)\rangle=-\langle\dot{\vec{M}}_I(t)\cdot\vec{M}_j(0)\rangle \tag{92}$$

For $t=0$ this last expression implies that the static correlation

$$\langle\vec{J}_j(0)\cdot\vec{M}_j(0)\rangle=0 \tag{93}$$

vanishes. Thus, one obtains as the generalization of Eq. (84)

$$(\epsilon_i(\omega)-1)\frac{2\epsilon_{EW}^{eff}+1}{2\epsilon_{EW}^{eff}+\epsilon(\omega)}=\frac{4\pi}{3}\frac{1}{Vk_bT}\times L\left[-\dot{\Phi}_i+\langle\vec{M}_i(0)\cdot\vec{J}_I(t)\rangle\right] \quad (94)$$

Finally, the relation between current and dipole moment of ionic components (Eq. (89)) helps in deriving the generalized constitutive relation

$$\vec{P}(\omega)=\Sigma(\omega)\vec{E}(\omega) \quad (95)$$

for the global, generalized DC or conductivity

$$\Sigma(\omega)=\frac{4\pi i}{\omega}\sigma(\omega)+\sum_i(\epsilon_i(\omega)-1) \quad (96)$$

that is appropriate for this case.

References

[1] M.K. Gilson, B.H. Honig, Proteins 4 (1988) 7.
[2] B. Honig, A. Nicholls, Science 268 (1995) 1144.
[3] M. Schaefer, M. Karplus, J. Chem. Phys. 100 (1996) 1578.
[4] D. Beglow, B. Roux, Biopolymers 35 (1995) 171.
[5] J. Tomasi, R. Bonaccorsi, R. Cammi, F.J. Olivares del Valle, J. Mol. Struct. 234 (1991) 401.
[6] B. Wang, G.P. Ford, J. Chem. Phys. 97 (1992) 4162.
[7] C.J. Cramer, D.G. Truhlar, J. Comput-Aided Mol. Design 6 (1992) 629.
[8] M.J. Field, P.A. Bash, M. Karplus, J. Comput. Chem. 11 (1990) 700.
[9] T. Simonson, C.F. Wong, A.T. Bünger, J. Phys. Chem. 101 (1997) 1935.
[10] P.L. Cummins, J.E. Gready, J. Comput. Chem. 19 (1998) 977.
[11] C.J. Cramer, D.G. Truhlar, J. Am. Chem. Soc. 113 (1991) 8305.
[12] C.J. Cramer, D.G. Truhlar, Science 256 (1992) 213.
[13] P.E.M. Siegbhan, R.H. Crabtree, Mol. Phys. 89 (1996) 279.
[14] D. Bakowies, W. Thiel, J. Chem. Phys. 100 (1996) 10580.
[15] S.W. de Leeuw, J.W. Perram, E.R. Smith, Proc. R. Soc. Lond. A 373 (1980) 27.
[16] M.P. Allen, D.J. Tidesley, Computer Simulations of Liquids, Oxford University Press, New York, 1989.
[17] M. Perutz, Science 201 (1978) 1187.
[18] Y. Yim, I. Muegge, A. Warshel, Biophys. J. 74 (1998) 1744.
[19] G. King, F.S. Lee, A. Warshel, J. Chem. Phys. 95 (1991) 4366.
[20] P.E. Smith, R.M. Brunne, A.E. Mark, W.F. van Gunsteren, J. Phys. Chem. 97 (1993) 2009.
[21] T. Simonson, D. Perahia, A.T. Brünger, Biophys. J. 59 (1991) 670.
[22] T. Simonson, D. Perahia, Proc. Natl. Acad. Sci. U.S.A. 92 (1995) 1082.
[23] T. Simonson, D. Perahia, J. Am. Chem. Soc. 117 (1995) 7987.
[24] T. Simonson, C.L. Brooks III, J. Am. Chem. Soc. 118 (1996) 8452.
[25] L. Yang, S. Weerasinghe, P.E. Smith, B.M. Pettitt, Biophys. J. 69 (1995) 1519.
[26] L. Yang, C.V. Valdeavella, D.H. Blatt, B.M. Pettitt, Biophys. J. 71 (1996) 3022.
[27] G. Löffler, H. Schreiber, O. Steinhauser, J. Mol. Biol. 270 (1997) 520.
[28] I.N. Levine, Quantum Chemistry, Chap. 14.4, 4th ed., Prentice Hall, Englewood Cliffs, 4th ed., 1991.
[29] J.D. Jackson, Classical Electrodynamics, 2nd ed., Wiley, New York, 1975.
[30] M. Born, R. Oppenheimer, Ann. Phys. 84 (1927) 457.
[31] R. Feynmann, Phys. Rev. 56 (1939) 340.
[32] A. Szabo, N.S. Ostlund, Modern Quantum Chemistry, McGraw-Hill, New York, 1989.
[33] R.G. Parr, W. Yang, Density Functional Theory of Atoms and Molecules, Clarendon Press, Oxford, 1989.
[34] P. Pulay, Mol. Phys. 17 (1969) 197.
[35] W. van Gunsteren, H. Berendsen, The GROMOS User Manual, Groningen, 1986.
[36] W.D. Cornell, et al., J. Am. Chem. Soc. 117 (1995) 5179.
[37] A. MacKerell, Jr., et al., J. Phys. Chem. B 102 (1998) 3586.
[38] B.J.C. Cabral, J.L. Rivali, B. Bigot, J. Chem. Phys. 86 (1987) 1467.
[39] P. Ahlström, A. Wallqvist, S. Engström, B. Jönsson, Mol. Phys. 68 (1989) 563.
[40] O. Steinhauser, S. Boresch, H. Bertagnoli, J. Chem. Phys. 93 (1990) 2357.
[41] W.H. Orrtung, Ann. N.Y. Acad. Sci. 303 (1977) 22.
[42] J. Warwicker, H.C.J. Watson, J. Mol. Biol. 157 (1982) 671.
[43] R.J. Zauhar, R.S.J. Morgan, J. Comput. Chem. 9 (1988) 171.
[44] C. Lim, D. Bashford, M. Karplus, J. Phys. Chem. 95 (1991) 5610.
[45] S. Tomac, A. Gräslund, J. Comput. Chem. 19 (1988) 893.
[46] P.A. Madden, D. Kivelson, Adv. Chem. Phys. 56 (1984) 467.
[47] F. Figuerido, G.S.D. Buono, R.M. Levy, J. Chem. Phys. 103 (1995) 6133.
[48] U. Essman, et al., J. Chem. Phys. 103 (1995) 8577.
[49] C.L. Brooks III, Curr. Opin. Struct. Biol. 5 (1995) 211.
[50] S. Boresch, O. Steinhauser, Ber. Bunsen Ges. 101 (1997) 1019.

[51] M. Neumann, O. Steinhauser, Chem. Phys. Lett. 102 (1983) 508.
[52] M. Neumann, O. Steinhauser, Chem. Phys. Lett. 95 (1983) 417.
[53] O. Steinhauser, Chem. Phys. 79 (1983) 465.
[54] J.A. Barker, R.O. Watts, Mol. Phys. 26 (1973) 789.
[55] W.L. Jorgensen, J. Chandrasekhar, J.D. Madura, J. Chem. Phys. 79 (1983) 926.
[56] E. Neria, S. Fischer, M. Karplus, J. Chem. Phys. 105 (1996) 1902.
[57] C. Chipot, C. Millot, B. Maigret, P.A. Kollman, J. Chem. Phys. 101 (1994) 7953.
[58] T. Simonson, Chem. Phys. Lett. 250 (1996) 450.
[59] P. Höchtl, S. Boresch, W. Bitomsky, O. Steinhauser, J. Chem. Phys. 109 (1988) 4927.
[60] M. Neumann, O. Steinhauser, G.S. Pawlay, Mol. Phys. 52 (1984) 97.
[61] H. Schreiber, O. Steinhauser, Chem. Phys. 168 (1992) 75.
[62] R. Abseher, H. Schreiber, O. Steinhauser, Prot.: Strut. Funct. Genet. 25 (1996) 366.
[63] R.M. Brunne, E. Liepinsh, G. Otting, K. Wüthrich, W.F. van Gunsteren, J. Mol. Biol. 231 (1993) 1040.
[64] P. Procacci, R. Scateni, Int. J. Quantum Chem. 42 (1992) 1515.
[65] M. Gerstein, J. Tsai, M. Levitt, J. Mol. Biol. 249 (1995) 955.
[66] M.F. Summers, T.L. South, B. Kim, D.R. Hare, Biochemistry 29 (1990) 329.
[67] H.J.C. Berendsen, J.R. Grigera, T.P. Straatsma, J. Phys. Chem. 91 (1987) 6269.
[68] Y. Harpaz, M. Gerstein, C. Chothia, Structure 2 (1994) 641.
[69] J.-P. Hansen, I.R. McDonald, Theory of Simple Liquids, Academic Press, London, New York, San Francisco, 1976.
[70] C.M. Cortis, J. Chem. Phys. 105 (1996) 5472.
[71] D. Levesque, J.M. Caillol, J.J. Weiss, J. Phys.: Condens. Matter 2 (1990) SA143.
[72] H. Frölich, Theory of Dielectrics. Dielectric Constant and Dielectric Loss, 2nd ed., Oxford, 1958.